Mon. Not. R. Astron. Soc. **360,** 416–446 (2005) doi:10.1111/j.1365-2966.2005.09057.x

Infrared mergers and infrared quasi-stellar objects with galactic winds – III. Mrk 231: an exploding young quasi-stellar object with composite outflow/broad absorption lines (and multiple expanding superbubbles)

S. Lípari,[1⋆] R. Terlevich,[2,3] W. Zheng,[4] B. Garcia-Lorenzo,[5] S. F. Sanchez[5,6] and M. Bergmann[7]

[1]*Córdoba Observatory and CONICET, Laprida 854, 5000 Córdoba, Argentina*
[2]*Institute of Astronomy, Madingley Road, Cambridge CB3 0HA*
[3]*Instituto Nacional de Astrofisica Optica y Electronica (INAOE), Puebla, Mexico*
[4]*Department of Physics and Astronomy, John Hopkins University, Baltimore MD 21218, USA*
[5]*Instituto de Astrofisica de Canarias, 38205 La Laguna, Tenerife, Canary Island, Spain*
[6]*Calar Alto Observatory, C/Jesus Durban Remon 2-2, E-04004 Almeria, Spain*
[7]*National Optical Astronomy Observatories Gemini Science Center, La Serena, Chile*

Accepted 2005 March 31. Received 2005 March 24; in original form 2005 January 11

ABSTRACT

We present a study of outflow (OF) and broad absorption line (BAL) systems in Mrk 231, and in similar infrared (IR) quasi-stellar objects (QSOs). This study is based mainly on one-dimensional and two-dimensional spectroscopy (obtained at La Palma/William Herschel Telescope, *Hubble Space Telescope*, *International Ultraviolet Explorer*, European Southern Observatory/New Technology Telescope, Kitt Peak National Observatory, Apache Point Observatory and Complejo Astronomico El Leoncito observatories) plus *Hubble Space Telescope* images. For Mrk 231, we report evidence that the extreme nuclear OF process has at least three main components on different scales, which are probably associated with: (i) the radio jet, at parsec scale; (ii) the extreme starburst at parsec and kiloparsec scale. This OF has generated at least four concentric expanding superbubbles and the BAL systems.

Specifically, inside and very close to the nucleus the two-dimensional spectra show the presence of an OF emission bump in the blend Hα+[N II], with a peak at the same velocity of the main BAL-I system ($V_{\rm Ejection\,BAL-I} \sim -4700$ km s^{-1}). This bump was more clearly detected in the area located at 0.6–1.5 arcsec (490–1220 pc), to the south-west of the nucleus core, showing a strong and broad peak. In addition, in the same direction [at position angle (PA) $\sim -120^{\circ}$, i.e. close to the PA of the small-scale radio jet] at 1.7–2.5 arcsec, we also detected multiple narrow emission-line components, with 'greatly' enhanced [N II]/Hα ratio (very similar to the spectra of jets bow shocks). These results suggest that the BAL-I system is generated in OF clouds associated with the parsec-scale jet.

The *Hubble Space Telescope* images show four (or possibly five) nuclear superbubbles or shells with radii $r \sim 2.9$, 1.5, 1.0, 0.6 and 0.2 kpc. For these bubbles, the two-dimensional Hα velocity field map and two-dimensional spectra show the following. (i) At the border of the more extended bubble (S1), a clear expansion of the shell with blueshifted velocities (with circular shape and at a radius $r \sim 5.0$ arcsec). This bubble shows a rupture arc – to the south – suggesting that the bubble is in the blowout phase. The axis of this rupture or ejection (at PA $\sim 00^{\circ}$) is coincident with the axis of the intermediate and large-scale structures detected at radio wavelengths. (ii) In addition, in the three more external bubbles (S1, S2, S3), the two-dimensional William Herschel Telescope spectra show multiple emission-line components with OF velocities, of $\langle V_{\rm OF\,Bubble}\rangle$ S1, S2 and S3 = $[-(650 - 420) \pm 30]$, $[-500 \pm 30]$ and $[-230 \pm 30]$ km s^{-1}. (iii) In the whole circumnuclear region ($1.8 < r < 5$ arcsec), the [N II]/Hα and [S II]/Hα narrow emission-line ratios show high values (>0.8), which are consistent with

⋆E-mail: sllipari@yahoo.com

low-ionization nuclear emission-line region/OF processes associated with fast velocity shocks. Therefore, we suggest that these giant bubbles are associated with the large-scale nuclear OF component, which is generated – at least in part – by the extreme nuclear starburst: giant supernova/hypernova explosions.

The variability of the short-lived BAL-III Na I D system was studied, covering almost all the period in which this system appeared (between ∼1984 and 2004). We have found that the BAL-III light curve is clearly asymmetric with a steep increase, a clear maximum and an exponential fall (similar to the shape of a supernova light curve). The origin of this BAL-III system is discussed, mainly in the framework of an extreme explosive event, probably associated with giant supernova/hypernova explosions.

Finally, the IR colour diagram and the ultraviolet BAL systems of IR + GW/OF + Fe II QSOs are analysed. This study shows two new BAL IR QSOs and suggests/confirms that these objects could be nearby young BAL QSOs, similar to those detected recently at $z \sim 6.0$. We propose that the phase of young QSOs is associated with accretion of a large amount of gas (by the supermassive black hole) + extreme starbursts + extreme composite OFs/BALs.

Key words: ISM: bubbles – ISM: jets and outflows – galaxies: individual: Mrk 231 – galaxies: kinematics and dynamics – quasars: general – galaxies: starburst.

1 INTRODUCTION

An important issue in astrophysics and cosmology is the study of extreme star formation and galactic winds/outflows (GWs/OFs), in mergers and quasi-stellar objects (QSOs) and their relation to the early phases of the formation of galaxies and active galactic nuclei (AGNs; see for references Aguirre et al. 2001; Scannapieco, Thacker & Davies 2001; Theuns et al. 2002; Lípari et al. 2004a,b,c,d).

1.1 Luminous infrared galaxies, mergers and active galactic nuclei

Luminous and ultraluminous infrared (IR) galaxies [LIRGs ($L_{\rm IR} \geqslant 10^{11}$ L$_\odot$) and ULIRGs ($L_{\rm IR} \geqslant 10^{12}$ L$_\odot$), respectively] are dusty, strong IR emitters where frequently a strong enhancement of star formation is taking place (for references, see Lípari et al. 2004a,b,c,d). Imaging surveys of LIRGs and ULIRGs show that a very high proportion (∼70–95 per cent) are mergers or interacting systems (Joseph & Wright 1985; Rieke et al. 1985; Sanders et al. 1988a; Melnick & Mirabel 1990; Clements et al. 1996). In LIRGs, there is a clear increase of the nuclear activity with the increase of IR luminosity (Sanders et al. 1988a,b; Veilleux, Kim & Sanders 1999, 2002b).

Strong evidence indicates that virtually all luminous IRAS galaxies are rich in interstellar gas, which is highly concentrated in their nuclei (Sanders et al. 1987, 1988a; Sanders, Scoville & Soifer 1991; Scoville et al. 1991). Specifically, there are observational evidence and theoretical works suggesting that in IR mergers and IR QSOs tidal torque and loss of angular momentum drive a large amount of interstellar gas into the central regions, leading to extreme starburst processes and probably fuelling a supermassive black hole (SMBH; for references, see Lípari et al. 2004a,d).

An important, common phenomenon associated with IR galaxies is the GW. We have found observational evidence for GW features from starbursts and/or AGNs in luminous IR systems (see, for references, Lípari et al. 2004a,b,c,d).

1.2 Galactic winds (associated with starbursts and active galactic nuclei)

GWs and OFs have been observed mainly in starburst and Seyfert galaxies (see Heckman, Armus & Miley 1990; Heckman et al. 2000; Cecil, Ferruit & Veilleux 2002; Veilleux et al. 2002a, 1994; Lípari, Colina & Macchetto 1994; Lípari et al. 2000b, 2003, 2004a,b,c,d). There is substantial theoretical literature about GWs associated with both processes: starbursts (Larson 1974; Ostriker & Cowie 1981; Chevalier & Clegg 1985; Ikeuchi & Ostriker 1986; Tomisaka & Ikeuchi 1988; Norman & Ikeuchi 1989; Suchkov et al. 1994; Strickland & Stevens 2000, and others) and with AGNs (for references, see Veilleux et al. 2002a).

There is clear evidence of galactic – and local – winds, shells, arcs and bubbles generated by multiple supernova (SN) explosions and massive star winds in starbursts. Our understanding of the main phases of GWs associated with starbursts was improved significantly by the use of theoretical and numerical models (see Tomisaka & Ikeuchi 1988; Mac Low, McCray & Norman 1989; Suchkov et al. 1994; Strickland & Stevens 2000). In general, good agreement has been found between these models and the observations.

On the other hand, for GWs associated with AGNs the situation is more complex, and very different models are proposed in order to explain the observed data. In these models, the OF could be generated by jet-driven thermal winds, accretion disc winds, X-ray heated torus winds, etc. (see Cappeti 2002; Cecil et al. 2002; Veilleux et al. 2002a; Morganti et al. 2003).

However, there is increasing evidence that nuclear galactic jets are one of the main sources of OFs in QSOs/AGNs (Cappeti 2002; Cecil et al. 2002; Veilleux et al. 2002a). In particular, there is clear detection and evidence of the interaction of jets with various phases of the interstellar medium (ISM), including the narrow-line region.

1.3 Infrared mergers with galactic winds

IR mergers often show strong starbursts with powerful OFs and GWs (Lípari et al. 2003, 2004a,b,c,d). Comparing our OF data base of IR mergers/QSOs (Lípari et al. 2004a, see their table 1) with two samples of nearby IR mergers, we found in both samples a

high proportion of mergers with GWs: ∼75 per cent. These results suggest (or confirm) that: (i) GWs are 'frequent events' in IR mergers and (ii) extreme starbursts + GW and extreme IR emission could be simultaneous processes, induced by merger events.

The low-velocity OF process (LVOF, $V_{\rm LVOF} < 700$ km s^{-1}; see Lípari et al. 2003, 2004a,b) observed in NGC 3256, 2623, 4039, 5514, etc. – using two-dimensional (2D) spectroscopy – is consistent with those found previously in Arp 220, Mrk 266, NGC 1614, NGC 3690, and other IR mergers with massive starbursts. In addition, we found an interesting fact: starbursts and low-ionization nuclear emission-line regions (LINERs) are the main sources of ionization in 'low-velocity OF' IR mergers (Lípari et al. 2000b, 2003, 2004a).

1.4 Infrared quasi-stellar objects with galactic winds

Recently, for IR QSOs we found the following. (i) Extreme velocity OF (EVOF, $V_{\rm EVOF} > 700$ km s^{-1}) objects with a composite nuclear source: starbursts + AGNs/QSOs; e.g. in Mrk 231, IRAS 19254−7245, 01003−2230, 13218+0552, 11119+3257, 14394+5332, and others (Lípari et al. 2003, 2004a,d). (ii) High-resolution *Hubble Space Telescope* (*HST*) Wide Field Planetary Camera 2 (WFPC2) images of IR + BAL + Fe II QSOs show in practically all of these objects giant arcs or shell features probably associated with OF or merger processes (Lípari et al. 2003).

In addition, using our data base of GWs/OFs in IR mergers/QSOs we found that in all the IR QSO candidates the Hβ broad-line component is blueshifted in relation to the narrow one, which is clearly consistent with the result obtained from the study of strong Fe II + BAL emitters, by Boroson & Meyers (1992). They proposed that blueshifted offset/asymmetry detected in the Hα broad components – of IR QSOs with strong Fe II + BAL systems – is probably due to the emission of the outflowing material, associated with the BAL process.

1.5 Broad absorption lines in infrared mergers/quasi-stellar objects

Some of the results obtained for nearby BAL QSOs, such as strong IR and Fe II emission, strong blue asymmetry/OF in Hα, radio quietness and very weak [O III]λ5007 emission (Low et al. 1989; Boroson & Meyers 1992; Lípari, Terlevich & Macchetto 1993; Lípari et al. 1994, 2003; Lípari 1994; Turnshek et al. 1997), can be explained in the framework of the starburst + AGN scenario. In our study of Mrk 231 and IRAS 0759+6559 (the nearest extreme IR + GW/OF + Fe II + BAL systems), we detected typical characteristics of young-starburst QSOs. In our evolutive model for young and composite IR QSOs (see, for references, Lípari 1994) we suggested that BAL systems could be linked to violent supermassive–starburst + AGN, which can lead to large-scale expanding supergiant shells, often obscured by dust. Several authors have suggested that this evolutive model shows good agreement with the observations (see Canalizo & Stockton 1997; Lawrence et al. 1997; Canalizo, Stockton & Roth 1998).

1.6 Possible links between infrared mergers and infrared quasi-stellar objects

The luminosities and space densities of ULIRGs in the local Universe are similar to those of QSOs (Soifer, Houck & Neugebauer 1987). In addition, at the highest IR luminosities, the presence of AGNs (and mergers) in LIRGs becomes important. Thus, LIRGs probably represent an important stage in the formation of QSOs and elliptical galaxies. These results strongly suggest that it is important to perform detailed studies of possible links among mergers, ULIRGs, QSOs and elliptical galaxies (Toomre & Toomre 1972; Toomre 1977; Larson 1974; Schweizer 1980, 1982; Joseph & Wright 1985; Sanders et al. 1988a,b; Lípari et al. 1993, 1994, 2003; Sanders & Mirabel 1996; Genzel et al. 1998, 2001; Colina et al. 2001; Tacconi et al. 2002).

Furthermore, the important detection of a correlation between the mass of galactic bulges and the mass of SMBHs is a confirmation that the formation and evolution of galaxies (bulges/ellipticals, mergers) and SMBHs (AGNs and QSOs) are physically related to one another (Kormendy & Richstone 1995; Magorrian et al. 1998; Ferrarese & Merrit 2000; Gebhardt et al. 2000; Kormendy 2000; Merrit & Ferrarese 2001).

In the last years, several possible links between mergers, starbursts, IR QSOs and ellipticals have been proposed. Specifically, Joseph et al., Sanders et al. and Lípari et al. have suggested three complementary sequences and evolutive links:

(i) merger → giant shocks → superstarbursts + GWs → elliptical galaxies;

(ii) merger → H_2-inflow (starbursts) → cold ULIRGs → warm ULIRGs + QSOs;

(iii) merger/s → extreme starburst + GW (inflow + outflow) → IR + Fe II + BAL composite/transition QSOs → standard QSOs and ellipticals → ?

Recently, several studies have confirmed the composite nuclear nature and the presence of merger and GW features in IR QSOs. In particular, Lípari et al. (2003, 2004a,d) found kinematical and morphological evidence of GWs in nearby 'IR + Fe II + BAL QSOs'.

2 PROGRAMME AND OBSERVATIONS

2.1 Programme

2.1.1 Infrared mergers/quasi-stellar objects with galactic winds (the main programme)

A current key issue in astrophysics is to explore the evolution of the star formation process, especially at high redshift, when the galaxies/QSOs formed, and where it is expected that the star formation rate is very high. With these aims in mind we began a project to study nearby star-forming + GW galaxies and distant Lyα emitters (see Lípari et al. 2004a,b,c,d). The first step in this project is to understand the star formation process in nearby galaxies because we can obtain more detailed and unambiguous information. Thus, our groups started a study of nearby IR mergers/QSOs, which are an excellent laboratory – at low redshift – for the analysis of extreme star formation and GW processes.

This study is based mainly on integral field spectroscopy, obtained at the Gemini, European Northern Observatory (ENO, La Palma–Spain), European Southern Observatory (ESO, Chile), Complejo Astronomico El Leoncito (CASLEO, Argentina) and Bosque Alegre (BALEGRE, Argentina) observatories, with the 8.1-m, 4.2-m, 3.6-m, 2.15-m and 1.5-m telescopes, respectively. The characteristics and goals of the programme have been described in detail by Lípari et al. (2004a). In particular, the main goal of this programme (at low redshift) is to analyse in detail the properties of the different stages of extreme starbursts, GWs, mergers, QSOs and elliptical galaxies (and their inter-relations).

In the present paper, we present new results from our programme of study of 'nearby' IR mergers/QSOs with GWs (see Table 1) for Mrk 231.

2.1.2 Broad absorption lines in IR + GW + Fe II mergers/quasi-stellar objects

A study and search of ultraviolet (UV) and optical BAL systems in extreme IR + GW/OF + Fe II QSOs have been started since 1993 (see Lípari 1994; Zheng et al., in preparation), using mainly *International Ultraviolet Explorer* (*IUE*) and *HST* UV spectra, plus ESO New Technology Telescope (NTT), Kitt Peak National Observatory (KPNO), Apache Point Observatory (APO) and CASLEO optical data. In general, the role of BALs in IR + GW/OF + Fe II QSOs/mergers must be carefully considered, for the following reasons. (i) Low et al. (1989) and Boroson & Meyers (1992) found that IR-selected QSOs show a 27 per cent low-ionization BAL QSO fraction compared with 1.4 per cent for the optically selected high-redshift QSO sample (Weymann et al. 1991). (ii) Extreme IR galaxies (ULIRGs) are mainly mergers (see Section 1). (iii) Very recently, Maiolino et al. (2004a) reported also a high fraction of BAL QSOs at very high redshift ($z \sim 6$). The high per cent of occurrence of broad absorption in extreme IR + GW/OF + Fe II QSOs/mergers may signal a fundamental relation (rather than merely a coincidence), and deserves detailed studies.

Lípari et al. (1993, 1994, 2003, 2004a,d), Scoville & Norman (1995), Egami et al. (1996), Lawrence et al. (1997) and others proposed that the extreme IR + GW/OF + Fe II + BAL phenomena are related – at least in part – to the end phase of an 'extreme–starburst + AGN' and the associated 'powerful bubble/GW'. At the final stage of a strong starburst, i.e. Type II SN phase [(8–60) $\times$ 10^6 yr from the initial burst; Norman & Ikeuchi 1989; Terlevich et al. 1992; Suchkov et al. 1994] giant galactic arcs and extreme Fe II + BAL systems can appear.

Specifically, the search of UV BALs was focused mainly in the IR objects of our data base of IR + GW/OF + Fe II QSOs/mergers (see Table 1), and we studied mainly the redshifted lines, C IVλ1549 and Mg II (plus Lyα, Si IV). Lípari (1994) reported a first study of the UV BAL systems in IRAS 0759+651, with projected ejection velocity of about 10 000 km s^{-1}. Previously, UV BAL systems were also reported in Mrk 231 (IRAS 12540+5708), IRAS 17002+5153 and IRAS 14026+4341.

It is important to note that in Table 1 several examples clearly show the consistency of the OF data presented. In particular, for IRAS F05024−1941, our study of EVOF in the ULIRG 1-Jy sample (using 'emission' lines), we found that this object is a candidate to EVOF, with a velocity close to −1500 km s^{-1} (Lípari et al. 2000b). From a study of narrow 'absorption' lines Rupke, Veilleux & Sanders (2002) obtained for this object an OF value of −1600 km s^{-1}. We have verified that for Mrk 231 the results using the offset method (by Zheng et al. 2002) gave the same value of OF (−1100 km s^{-1}) as that already obtained from the detection of two emission-line systems in [O II]λ3727 (by Lípari et al. 1994). A similar agreement between the values of the OF obtained from multiple emission lines (Lípari et al. 2000b) and the offset method (Zheng et al. 2002) was found, for the cases of IRAS 11119+3257 and IRAS 15462−0450 (see Table 1).

In this paper, we report on new results from this programme, in particular, the detection of two new IR + GW/OF + Fe II QSOs with BAL systems: IRAS 21219−1757 and IRAS 04505−2958.

2.2 Mrk 231: the nearest extreme IR + GW + BAL + Fe II merger/quasi-stellar object (of the programme)

Since Mrk 231 was discovered (by its strong UV continuum; Markarian 1969) it has been extensively studied and has been recognized as a remarkable galaxy. It is the most luminous galaxy in the local Universe ($z < 0.1$), the nuclear spectrum shows extreme broad emission lines and strong BAL systems, and the morphology is associated with a merger, etc. (Arakelian et al. 1971; Adams 1972; Adams & Weedman 1972; Rieke & Low 1972, 1975; Boksenberg et al. 1977, and others). It is important to remark that Sanders et al. (1987), Bryant & Scoville (1996) and Downes & Solomon (1998) found a very high concentration of CO molecular gas in the nuclear region of Mrk 231 (3×10^9 M$_\odot$, within a diameter of 1.0 arcsec, ∼814 pc).

Before the *IRAS* was launched, Mrk 231 was known to have an extreme IR luminosity with $M_K = -24.7$ (Rieke & Low 1972, 1975; Cutri, Rieke & Lebofsky 1984). Even after *IRAS* has expanded the known population of ULIRGs, Mrk 231 has remained one of the most luminous objects in the local Universe, with $L_{\rm IR(8-1000\ \mu m)} = 3.56 \times 10^{12}$ L$_\odot$ and $L_{\rm IR}/L_B = 32$. Consequently, the bolometric luminosity (dominated by the continuum IR emission) places the nucleus of this IR merger among the QSOs. Weedman (1973) has already proposed that this extreme IR luminosity is associated with UV emission reradiated thermally – in the IR – by dust. The origin of the extreme IR luminosity of Mrk 231 is associated with the two main sources of nuclear energy: an AGN plus an extreme nuclear + circumnuclear starburst. In particular, Lípari et al. (1994) suggested that Mrk 231 is an evolving 'composite young IR QSO'.

Mrk 231 also shows very interesting spectral characteristics, dominated in the optical by extremely strong Fe II and broad Balmer emission lines at $Z_{\rm em} = 0.042$ (Arakelian et al. 1971; Adams & Weedman 1972; Boksenberg et al. 1977). In addition, it shows remarkable absorption-line systems: a clear stellar absorption at $Z_{\rm abs} = 0.042$ plus at least three strong BAL systems. These strong BAL systems show the following velocity of ejection: $V_{\rm eject}$ of BAL-I, BAL-II and BAL-III ∼4700, ∼6000 and ∼8000 km s^{-1}. The last BAL-III system suddenly appeared sometime between 1984 December and 1988 May (Boroson et al. 1991).

Thus, Mrk 231 is the nearest extreme IR + GW/OF + BAL + Fe II QSO. In this paper, new results of the OF process in Mrk 231 are reported. Throughout the paper, a Hubble constant of $H_0 = 75$ km s^{-1} Mpc^{-1} is assumed. For Mrk 231 we adopted the distance of ∼168 Mpc (cz= 12 465 ± 10 km s^{-1}, where cz is the standard light velocity × redshift), and thus the angular scale is 1 arcsec ≈814 pc.

2.3 La Palma/William Herschel Telescope + INTEGRAL two-dimensional spectroscopy

2D optical spectroscopy of Mrk 231 was obtained during a photometric night in 2001 April at the 4.2-m telescope at Observatorio Roque de los Muchachos on the Canary island of La Palma. The 4.2-m William Herschel Telescope (WHT) was used with the INTEGRAL fibre system (Arribas et al. 1998) and the WYFFOS spectrograph (Bingham et al. 1994). The seeing was approximately 1.0 arcsec.

INTEGRAL links the $f/11$ Naysmith focus of the WHT with the slit of WYFFOS via three optical fibre bundles. A detailed technical description of INTEGRAL is provided by Arribas et al. (1998); here, we only recall its main characteristics. The three bundles have different spatial configurations on the focal plane and can be interchanged depending the scientific programme or the seeing conditions. At the focal plane, the fibres of each bundles are arranged in two groups, one forming a rectangle and the other an outer ring (for collecting background light, in the case of small-sized objects). The data analysed in this paper were obtained with the standard bundle 2, which

Table 1. IR mergers and IR QSOs/AGN with low and high/extreme velocity OF.

Object	$V_{\rm OF\,1}$ km s^{-1}	z	$L_{\rm FIR}$ log $L/{\rm L}_{\odot}$	$L_{\rm IR}/L_B$	Nuclear activity	Morph type	RF	BAL	$\alpha_{60,25}$	$\alpha_{100,60}$	OF type	OF reference
Low-velocity OF												
Arp 220	−450	0.0183	12.18	87	L+SB	PM	–	–	−2.94	−0.16	EL	Heckman et al. (1987)
IRAS 00182−7112	−450	0.3270	12.90	200	L+SB	(M)	–	–	−2.51	+0.05	EL	Heckman et al. (1990)
IRAS 03250+1606	−431	0.1290	12.06	–	L	M	–	–	–	−0.49	AL	Rupke et al. (2002)
IRAS 03514+1546	−200	0.0210	11.10	–	SB	M	–	–	−2.32	−0.79	AL	Heckman et al. (2000)
IRAS 09039+0503	−656	0.1250	12.07	–	L	M	–	–	–	−0.65	AL	Rupke et al. (2002)
IRAS 11387+4116	−511	0.1490	12.18	–	SB	OM	–	–	–	−0.76	AL	Rupke et al. (2002)
IRAS 23128−5919	−300	0.0449	12.60	8	L+SB	M	–	–	−2.18	−0.03	EL	Lípari et al. (2000b)
Mrk 266	−300	0.0290	11.37	8	SB	PM	–	–	−2.14	−0.80	EL	Wang et al. (1997)
Mrk 273	−600	0.0385	12.14	36	L+SB	PM	–	–	−2.58	+0.03	EL	Colina, Arribas & Borne (1999)
NGC 1614	−400	0.0155	11.61	18	L+SB	M	–	–	−1.70	−0.02	EL	Ulrich (1972)
NGC 2623	−405	0.0185	11.55	17	L+SB	M	–	–	−2.96	−0.37	EL	Lípari et al. (2004d)
NGC 3256	−370	0.0094	11.57	9	SB	MM	–	–	−1.95	−0.52	EL	Lípari et al. (2000a)
NGC 3690	−300	0.0103	11.91	23	SB	PM	–	–	−1.71	−0.07	EL	Heckman et al. (1990)
NGC 4039	−365	0.0056	10.99	6	L+SB	PM	–	–	–	–	EL	Lípari et al. (2000b)
NGC 5514	−320	0.0245	10.70	1	L+SB	PM	–	–	−1.96	−1.14	EL	Lípari et al. (2004d)
Extreme OF												
IRAS 01003−2238	−770	0.1180	12.24	67	QSO+SB	OM	–	–	−1.42	+0.48	EL	Lípari et al. (2000b)
IRAS 05024−1941	−1150	0.1920	12.43	–	S2	M	–	–	−2.30	−0.47	EL	Lípari et al. (2000b)
IRAS 05024−1941	−1676	0.1920	12.43	–	S2	M	–	–	−2.30	−0.47	AL	Rupke et al. (2002)
IRAS 05189−2524	−849	0.0420	12.07	–	S2	M	–	–	−1.56	+0.36	AL	Rupke et al. (2002)
IRAS 10378+1108	−1517	0.1360	12.26	–	L	M	–	–	–	–	AL	Rupke et al. (2002)
IRAS 11119+3257	−1300	0.1885	12.64	–	S1+SB	M	1.12	–	−1.73	+0.80	EL	Lípari et al. (2000b)
IRAS 11119+3257	−950	0.1885	12.64	–	S1+SB	M	1.12	–	−1.73	+0.08	OSM	Zheng et al. (2002)
IRAS 13218+0552	−1800	0.2048	12.63	96	QSO+SB	OM	–	–	−1.22	+0.98	EL	Lípari et al. (2000b)
IRAS 14394+5332	−880	0.1050	12.04	–	S2	MM	–	–	−1.98	−0.40	EL	Lípari et al. (2000b)
IRAS 15130−1958	−780	0.1093	12.09	–	S2	M	–	–	−1.82	−0.36	EL	Lípari et al. (2000b)
IRAS 15462−0450	−1000	0.1001	12.16	–	S1	M	–	–	−2.13	−0.05	EL	Lípari et al. (2000b)
IRAS 15462−0450	−1110	0.1010	12.35	–	S1	M	1.32	–	−2.13	−0.05	OSM	Zheng et al. (2002)
IRAS 19254−7245	−800	0.0597	12.04	30	QSO+SB	PM	–	–	−1.70	−0.11	EL	Colina et al. (1991)
Mrk 231	−1000	0.0422	12.53	32	QSO+SB	M	1.83	Yes	−1.49	+0.11	EL	Lípari et al. (1994)
Mrk 231	−1100	0.0422	12.53	32	QSO+SB	M	1.83	Yes	−1.49	+0.11	OSM	Zheng et al. (2002)
NGC 3079	−1600	0.0040	10.49	2	L+SB	Sp	–	–	−3.01	−1.41	EL	Heckman et al. (1990)
NGC 6240	−930	0.0243	11.83	15	L+SB	PM	–	–	−2.16	−0.40	EL	Heckman et al. (1990)
IR QSO offset-OF												
IRAS 00275−2859	−730	0.2792	12.64	9	QSO+SB	PM	1.47	–	−1.58	−0.12	OSM	Zheng et al. (2002)
IRAS 00509+1225	−1110	0.0600	11.87	20	QSO+SB	PM	1.40	–	−0.70	−0.32	OSM	Lípari et al. (2004d)
IRAS Z01373+0604	−1660	0.3964	12.30	3	QSO+SB	–	2.33	–	−0.50	−1.59	OSM	Lípari et al. (2004d)
IRAS 02054+0835	−1355	0.3450	12.97	–	QSO	–	2.42	–	–	–	OSM	Zheng et al. (2002)
IRAS 02065+4705	−500	0.1320	12.27	–	QSO	–	1.65	–	−1.96	–	OSM	Zheng et al. (2002)
IRAS 04415+1215	−875	0.0890	12.41	–	QSO	–	1.74	–	–	–	OSM	Zheng et al. (2002)
IRAS 04505−2958	−1700	0.2863	12.55	20	QSO+SB	PM	1.33	Yes	−1.41	−0.32	OSM	Lípari et al. (2004d)
IRAS 06269−0543	−550	0.1170	12.49	–	QSO	–	0.57	–	−1.36	+0.19	OSM	Zheng et al. (2002)
IRAS 07598+6508	−2030	0.1483	12.45	5	QSO+SB	M	2.75	Yes	−1.32	−0.04	OSM	Zheng et al. (2002)
IRAS 07598+6508	−1920	0.1483	12.45	5	QSO+SB	M	2.75	Yes	−1.32	−0.04	OSM	Lípari et al. (2004d)
IRAS 09427+1929	−1640	0.2840	12.61	–	QSO	–	2.98	–	–	–	OSM	Zheng et al. (2002)
IRAS 10026+4347	−650	0.1780	12.20	–	QSO	–	2.07	–	−1.26	−0.88	OSM	Zheng et al. (2002)
IRAS Z11598−0112	−970	0.1510	11.91	–	QSO	–	1.71	–	–	–	OSM	Zheng et al. (2002)
IRAS 13305−1739	−730	0.1480	12.21	–	S2	OM	–	–	−1.24	+0.21	OSM	Lípari et al. (2004d)
IRAS 13342+3932	−920	0.1790	12.49	–	QSO	–	0.73	–	–	–	OSM	Zheng et al. (2002)
IRAS 13451+1232	−1210	0.1220	12.28	–	S2	PM	–	–	−1.20	−0.14	OSM	Lípari et al. (2004d)
IRAS 14026+4341	−1500	0.3200	12.55	40	QSO	M	1.12	Yes	−0.89	−0.92	OSM	Lípari et al. (2004d)
IRAS 17002+5153	−1050	0.2923	12.58	5	QSO+SB	PM	1.56	Yes	−0.65	−0.06	OSM	Lípari et al. (2004d)
IRAS 18508−7815	−1250	0.1620	12.00	8	QSO	M	2.40	–	−1.63	−0.84	OSM	Lípari et al. (2004d)
IRAS 20036−1547	−400	0.1930	12.70	–	QSO	–	2.74	–	–	–	OSM	Zheng et al. (2002)

consisted of 219 fibres, each of 0.9 arcsec in diameter in the sky. The central rectangle is formed by 189 fibres, covering a field of view of 16.4 × 12.3 arcsec^2, and the other 30 fibres form a ring 90 arcsec in diameter.

The WYFFOS spectrograph was equipped with a 1200 lines mm^{-1} grating, covering the range λλ6200–7600 Å. A TEX CCD array of 1124 × 1124 pixels of 24-μm size was used, giving a linear dispersion of about ∼1.45 Å pixel^{-1} (∼2.5 Å effective resolution,

Table 1 – *continued*

Object	V_{OF1} km s^{-1}	z	L_{FIR} log $L/L_{\odot}$	L_{IR}/L_B	Nuclear activity	Morph type	RF	BAL	$\alpha_{60,25}$	$\alpha_{100,60}$	OF type	OF reference
IRAS 20520−2329	−660	0.2060	12.52	–	QSO	–	2.02	–	–	−1.27	OSM	Zheng et al. (2002)
IRAS 21219−1757	−460	0.1100	11.98	89	QSO	OM	1.82	Yes	−1.00	−0.20	OSM	Lípari et al. (2004d)
IRAS 22419−6049	−390	0.1133	11.30	–	QSO+SB	M	–	–	−0.33	–	OSM	Lípari et al. (2004d)
IRAS 23389+0300	−1640	0.1450	12.09	–	S2	PM	–	–	–	+0.10	OSM	Lípari et al. (2004d)

Column 2 shows OF values obtained from the references included in column 13. Values between parentheses are possible detections. [O III] MC indicates emission line [O III]λ5007 with multiple components. In column 4, L_{IR} were obtained for [8–1000 μm], using the relation given by Sanders & Mirabel (1996). Column 6 shows the properties of the nuclear activity were obtained from Veilleux et al. (1999), Canalizo & Stockton (2001) and Lípari et al. (2003): S1 denotes Seyfert 1, S2 denotes Seyfert 2, L denotes Liners and SB denotes starburst. In column 7, for the morphological or interaction type we used the classification criteria of Veilleux et al. (2002b) and Surace (1998): PM denotes pre-merger, M denotes merger, OM denotes old merger, MM denotes multiple merger and Sp denotes spirals. In column 8, RF is the ratio of the emission line Fe IIλ4570/Hβ. In columns 10 and 11, α are the IR colour indexes, for three IR bands (for details see the text). The IR fluxes were obtained from the last IRAS and *ISO* catalogues and published data, using the NED. In column 12, EL, AL and OSM indicate OF derived from emission, absorption lines and the offset emission-line method, respectively (see the text)

∼100 km s^{-1}). With this configuration and pointing to the central region of Mrk 231, we took three exposures of 1800 s.

2.4 *HST* ACS, WFPC2 and NICMOS broad-band images

Near-UV *HST* Advanced Camera for Surveys (ACS) archival images of Mrk 231 were analysed, obtained with the High-Resolution Channel (HRC). They include images with the filter F330W (3354 Å, Δλ588 Å). The scale is 0.027 arcsec pixel^{-1}.

Optical *HST* WFPC2 observations were analysed, which include broad-band images positioned on the Planetary Camera chip with a scale of 0.046 arcsec pixel^{-1}, using the filters F439W (4283 Å, Δλ464 Å, ∼*B* Cousin filter) and F814W (8203 Å, Δλ1758 Å, ∼*I*).

HST Near-Infrared Camera and Multi-Object Spectrometer (NICMOS) archival data were studied, which include mainly images with the filter F160W (1.60 μm, Δλ0.4 μm), using camera 2 with a scale of 0.076 arcsec pixel^{-1}.

For details of the *HST* image observations, see also Table 2.

2.5 *HST* UV-FOS and UV-STIS one-dimensional spectroscopy

HST FOS aperture spectroscopy of the main optical nucleus of Mrk 231 was obtained, from the *HST* archive (at ESO Garching). The spectra were taken with the G190L (λλ1150–2300), G190H (λλ1575–2320) and G270H (λλ2225–3290) gratings and the blue detector. The G190H and G270H observations were made with the effective aperture of 4.3 × 1.4 arcsec^2, and these spectra have resolutions of ∼3 and 4 Å, FWHM, respectively. The G160L observations were made with the aperture of 1.0 arcsec, and the spectra have a resolution of ∼8 Å, FWHM.

In addition, *HST* FOS spectra of extreme IR + Fe II QSOs with GWs were analysed. These data were used in our study/search of UV–BAL systems (for details, see Table 2).

HST STIS long-slit spectra of IR + GW/OF + Fe II QSOs were obtained (mainly from the *HST* archive). The spectra were taken with the G160L and G140L gratings. The STIS CCD has a scale of 0.05 arcsec pixel^{-1}.

2.6 La Palma/Nordic Optical Telescope optical broad-band images

An optical *V* broad-band optical image of Mrk 231 was obtained during a photometric night in 1991 May at the 2.5-m Nordic Optical Telescope (NOT) at the Observatorio Roque de los Muchachos (on the Canary island of La Palma). A TEX CCD chip with scale 0.197 arcsec pixel^{-1} was used. The observations were carried out in excellent seeing conditions, with a value of 0.7 arcsec (FWHM).

2.7 KPNO long-slit one-dimensional spectroscopy

Optical long-slit spectra of Mrk 231 and IR + GW/OF + Fe II QSOs were obtained on the KPNO 2.15-m telescope with the Gold Cam spectrograph, by using two gratings of 300 grooves mm^{-1} (7 Å, ∼300 km s^{-1} resolution) covering the wavelength ranges 3350–5200 and 5100–7100 Å. The observations were taken during one photometric night in 1991 February (Table 2). The spectra were obtained with a slit width of 1.5 arcsec. The seeing was in the range 1.0–1.5 arcsec (FWHM).

The data of the *IRAS* 1-Jy ULIRG sample were obtained with the Gold Cam spectrograph on the KPNO 2.15-m telescope by using a grating of 300 grooves mm^{-1} (8-Å resolution) and covering the wavelength range 4500–9000 Å.

2.8 *IUE* one-dimensional spectroscopy

UV *IUE* spectra were obtained for our programme of searching UV–BAL systems in extreme IR + GW/OF + Fe II QSOs (Table 2). In addition, data from the *IUE* archival – of this type of object – were analysed. The *IUE* LWP and SWP spectra cover the wavelength ranges 1150–1980 and 1900–3290 Å, with a resolution of ∼8 Å (∼300 km s^{-1}).

2.9 ESO NTT and 3.6-m telescope spectra

The ESO Faint Object Spectrograph and Camera II (EFOSC II) on the 3.5-m NTT at La Silla was used to obtain long-slit spectra of IR + GW/OF + Fe II QSOs. These long-slit observations were taken during one photometric night in 1993 July (see Table 2). The spectra cover the wavelength range ∼3560–5200 Å, with a resolution of ∼7 Å (∼300 km s^{-1}).

The EFOSC on the 3.6-m telescope at La Silla was used to obtain long-slit spectra and high-resolution images. Medium-resolution spectra were obtained with the B150, O150 and R150 grisms, which provide a resolution of ∼7 Å in the wavelength range 3600–9800 Å (during three photometric nights in 1995 January and 1991 July; see Table 2).

2.10 APO one-dimensional spectroscopy

The APO spectra of IR GW/OF + Fe II QSOs were taken with the double imaging spectrograph (DIS) of the 3.5-m telescope. Optical long-slit observations were obtained during one photometric night in 2004 September (see Table 2). The medium-resolution spectra

Table 2. Journal of observations of Mrk 231 and similar extreme IR + GW/OF + Fe II QSOs.

Object	Date	Telescope/ instrument	Spectral region	Exposure time (s)	Comments
Mrk 231	2001 Apr 12	4.2-m WHT/INTEGRAL	λλ6200–7600 Å	1800×3	⟨FWHM⟩ = 1.0 arcsec
Mrk 231	1991 Feb 15	2.15-m KPNO/GoldCam	λλ3350–5200 Å	900×2	PA = 90°, slit width = 1.5 arcsec
		2.15-m KPNO/GoldCam	λλ5100–7100 Å	900×2	PA = 90°, slit width = 1.5 arcsec
Mrk 231	1991 May 11	2.5-m NOT	*V*	1200×3	⟨FWHM⟩ = 0.7 arcsec
Mrk 231	1992 Nov 27	*HST*/FOS	G190H, λλ1275–2320 Å	5760	archival
Mrk 231	1992 Nov 27	*HST*/FOS	G270H, λλ2225–3295 Å	2880	archival
Mrk 231	1996 Nov 21	*HST*/FOS	G160L, λλ1150–2300 Å	770	archival
Mrk 231	1995 Oct 23	*HST*/WFPC2	F439W, λλ4283/464 Å	2226	⟨FWHM⟩ = 0.1 arcsec, archival
Mrk 231	1995 Oct 23	*HST*/WFPC2	F814W, λλ8203/1758 Å	712	⟨FWHM⟩ = 0.1 arcsec, archival
Mrk 231	2003 Mar 17	*HST*/ACS	F330W, λλ3354/588 Å	1140	⟨FWHM⟩ = 0.1 arcsec, archival
Mrk 231	2003 Sep 09	*HST*/NICMOS	F160W, λλ1.60/0.40 μm	640	⟨FWHM⟩ = 0.22 arcsec, archival, NIC2
I21219−1757	1989 Jun 29	2.15-m CASLEO/Z-machine	λλ4700-7200 Å	1500×3	aperture: 3 × 6 arcsec^2
I21219−1757	1993 Jul 13	2.15-m CASLEO/UCS	λλ6500-7000 Å	1800×2	PA = 90° slit width= 2.0 arcsec
I21219−1757	1997 Mar 13	2.15-m CASLEO/UCS	λλ4000-7500 Å	1800×2	PA = 90° slit width= 1.5 arcsec
I21219−1757	1995 Oct 24	2.15-m KPNO/GoldCam	λλ4500–9000 Å	1800×2	PA = 90°, slit width = 1.5 arcsec
I21219−1757	1995 May 26	*IUE*/LWP30773	λλ1150–1980 Å	9000	UV BAL Programme
I21219−1757	1995 May 26	*IUE*/SWP54757	λλ1900–3290 Å	112000	UV BAL Programme
I21219−1757	1999 Jun 03	*HST*/STIS	G160L, λλ1150–1550 Å	2420	archival
I07598+6508	1991 Feb 15	2.15-m KPNO/GoldCam	λλ3350–5200 Å	1800×2	PA = 90°, slit width = 1.5 arcsec
I07598+6508	1991 Feb 15	2.15-m KPNO/GoldCam	λλ5100–7100 Å	1800×2	PA = 90°, slit width = 1.5 arcsec
I07598+6508	1998 Dec 10	*HST*/STIS	G140L, λλ1000–1400 Å	2570	archival
I07598+6508	1989 Sep 28	*IUE*/LWP16445	λλ1150–1980 Å	12000	archival
I07598+6508	1989 Sep 28	*IUE*/SWP37199	λλ1900–3290 Å	12840	archival
I07598+6508	1990 Dec 17	*IUE*/LWP19437	λλ1150–1980 Å	7800	archival
I07598+6508	1990 Dec 17	*IUE*/SWP40376	λλ1900–3290 Å	13200	archival
I14026+4341	1990 Sep 19	2.15-m KPNO/GoldCam	λλ4350–5700 Å	1800×2	PA = 90°, slit width = 1.5 arcsec
I14026+4341	1994 Jul 17	*HST*/FOS	G190H, λλ1570–2300 Å	978	archival
I14026+4341	1991 Jun 14	*IUE*/LWP20600	λλ1150–1980 Å	21360	archival
I14026+4341	1989 May 17	*IUE*/SWP36278	λλ1900–3290 Å	21300	archival
I17002+5153	1990 Sep 19	2.15-m KPNO/GoldCam	λλ4350–5700 Å	1800×2	PA = 90°, slit width = 1.5 arcsec
I17002+5153	1993 Mar 10	*HST*/FOS	G190H, λλ1600–2300 Å	2026	archival
I17002+5153	1984 Oct 18	*IUE*/LWP04596	λλ1150–1980 Å	51900	archival
I17002+5153	1985 Sep 14	*IUE*/LWP06655	λλ1150–1980 Å	21900	archival
I17002+5153	1984 Oct 16	*IUE*/SWP24185	λλ1900–3290 Å	50700	archival
I17002+5153	1984 Aug 11	*IUE*/SWP23672	λλ1900–3290 Å	24180	archival
I17002+5153	1984 AUG 15	*IUE*/SWP23691	λλ1900–3290 Å	24600	archival
I18508−7815	1991 Jul 15	3.6-m ESO/EFOSC	λλ3600–5590 Å	1800×2	PA = 90°, slit width = 1.5 arcsec
I18508−7815	1991 Jul 15	3.6-m ESO/EFOSC	λλ5050–7000 Å	1800×2	PA = 90°, slit width = 1.5 arcsec
I18508−7815	1991 Jul 15	3.6-m ESO/EFOSC	λλ6600–9800 Å	1800×2	PA = 90°, slit width = 1.5 arcsec
I18508−7815	1991 Jul 18	*IUE*/LWP20841	λλ1150–1980 Å	25200	archival
I18508−7815	1995 May 27	*IUE*/SWP54772	λλ1900–3290 Å	24300	UV BAL Prog.
PHL1092	1993 Jul 15	3.5-m ESO NTT	λλ3200–5000 Å	1500×3	PA=90,UV BAL Programme
PHL1092	2004 Sep 08	3.5-m APO DIS	λλ3500–5600 Å	1800×2	PA = 90°, slit width = 1.5 arcsec
PHL1092	2004 Sep 08	3.5-m APO DIS	λλ5300–10000 Å	1800×2	PA = 90°, slit width = 1.5 arcsec
I 04505−2958	1995 Sep 30	HST/WFPC2	F702W, λλ6895/1389 Å	1800	archival
I 04505−2958	1996 Nov 18	*HST*/FOS	G190H, λλ1570–2300 Å	1620	archival
I 04505−2958	1999 Dec 08	2.15-m CASLEO/UCS	λλ4300-7700 Å	1800×2	PA = 90° slit width= 1.5 arcsec

give an effective resolution of ∼8–10 Å (∼300 km s^{-1}), covering the two wavelength ranges λλ3500–5600 and 5300–10 000 Å. The seeing was ∼1.5 arcsec (FWHM).

2.11 CASLEO one-dimensional spectroscopy

Spectrophotometric observations of IR + GW/OF + Fe II QSOs were taken at CASLEO (San Juan, Argentina) with the 2.15-m Ritchey–Chrétien telescope. Optical long-slit and aperture spectroscopy observations were obtained during three photometric nights in 1989 June, 1993 July and 1997 March (see Table 2). Long-slit spectroscopic observations with medium resolution were obtained with the Columbia University spectrograph (UCS; e.g. Lípari, Tsvetanov & Macchetto 1997). The medium-resolution spectra were made using a 600 line mm^{-1} grating, a slit width of 2.5 arcsec, which gives an effective resolution of ∼6 Å (∼290 km s^{-1}) and a

dispersion of 120 Å mm^{-1}, covering the wavelength range λλ4000–7500 Å. Aperture spectroscopic data were obtained with the 'Z-machine' (e.g. Lípari, Macchetto & Golombeck 1991a; Lípari, Bonatto & Pastoriza 1991b). These aperture spectra were made using a 600 line mm^{-1} grating, giving a dispersion of 130 Å mm^{-1} and an effective resolution of ∼8 Å (∼300 km s^{-1}) covering the wavelength range λλ4700–7200. The seeing was in the range 1.5–2.5 arcsec (FWHM).

2.12 Reduction

The IRAF[1] software package was used to reduce and analyse the data. The reduction of the 2D spectroscopic observations consists of two main steps: (i) reduction of the spectra (for each of the 219 fibres); (ii) generation of 2D maps by interpolating the selected parameter (e.g. emission-line intensity, continuum intensity, radial velocity, etc.) from the grid values defined by the fibre bundle. Step (i) was basically done in the same way as for long-slit spectroscopy, including bias subtraction, aperture definition and trace, stray-light subtraction, the extraction of the spectra, wavelength calibration, throughput correction and cosmic-ray rejection. We obtained typical wavelength calibration errors of 0.1 Å, which give velocity uncertainties of 5 km s^{-1}. For step (ii) we used the software package INTEGRAL,[2] with 2D interpolation routines. In particular, we transformed ASCII files with the positions of the fibres and the corresponding spectral features, into regularly spaced standard FITS files. Maps generated in this way are presented in the next sections.

The IRAF and STSDAS[3] software packages were used to analyse the *HST*, ESO, *IUE*, KPNO, NOT, APO and CASLEO imaging and spectrophotometric data. The *HST* data were reduced at the Space Telescope Science Institute, using the standard process.

The emission-line components were measured and decomposed using Gaussian profiles by means of a non-linear least-squares algorithm described in Bevington (1969). In particular, we used the software SPECFIT[4] and SPLOT from the STSDAS and IRAF packages, respectively. An example of SPECFIT deblending, using three components for each emission line in IRAS 01003−2238, was shown in fig. 2 of Lípari et al. (2003). We note that in each WHT spectrum the presence of OF components and multiple emission-line systems were confirmed by detecting these systems in at least two or three different emission lines ([N II]λ6583, Hα, [N II]λ6548 and [S II]λλ6717/6731). For the study of the kinematics, the ADHOC[5] software package was also used.

3 RESULTS

This section focuses on presenting (for Mrk 231): (i) high-resolution *HST* near-UV, optical and near-IR images of the main body; (ii) 2D spectroscopy mainly for the central regions; (iii) one-dimensional (1D) spectroscopy for the nuclear region; (iv) a study of variability of the Na I D BAL-III system (based on 1D spectroscopy). In particular, we study the extreme nuclear OF with multiple expanding concentric supershells, giant shocks and BAL systems. In addition, new observations of UV–BAL systems in IR + GW/OF + Fe II QSOs are analysed.

3.1 Near-ultraviolet, optical and near-infrared *HST* and NOT images: multiple concentric nuclear superbubbles (and knots)

Here, we present a multiwavelength morphological study (using mainly high-resolution *HST* near-UV, optical and near-IR broad-band images) of the nuclear and circumnuclear structures of Mrk 231.

The NOT *V* image (Fig. 1) shows almost the whole merger. This galaxy consists of a nearly elliptical main body ($R \sim 10$ kpc) with a compact nucleus, plus two faint tidal tails (see also Hamilton & Keel 1987; Neff & Ulvestad 1988; Lípari et al. 1994). These are typical features observed in advanced mergers.

It is important to note that, previously, in the circumnuclear region of Mrk 231, Lípari et al. (1994) found clear evidence of a powerful nuclear GW, and they have proposed that this OF process (in part associated with a starburst) has generated the circumnuclear blue arc/shell (at $r \sim 3$ kpc, and to the south of the nucleus). However, Armus et al. (1994) have suggested that this arc is associated with an obscured second nucleus (they have also suggested that in this blue region or 'shell' there is no evidence of the star formation process). *HST* WFPC2 observations of Mrk 231 confirmed that this blue arc is a 'dense supershell of star-forming knots' (see Surace et al. 1998; Lípari et al. 2003). In the next sections we will expand these previous studies.

3.1.1 Multiple concentric nuclear superbubbles/shells

Figs 2(a)–(d) present high-resolution *HST* broad-band images obtained in the near-UV, optical and near-IR wavelengths through the filters F330W (∼ *U*), F439W (∼ *B*), F814W (∼ *I*) and F160W (∼ *H*). These original *HST* images (without any smooth or filtering process) clearly show four concentric supergiant galactic shells or bubbles with the centre in the nucleus and showing several bright knots. Then, in order to analyse in detail the structure of these shells, a basic study was performed, following the good results obtained using the filtering technique in the study of the morphology and kinematics of NGC 2623 and 5514 (Lípari et al. 2004a,d). Figs 3(a)–(d) were obtained from the subtraction of a smooth image (for each filter) of the main body of Mrk 231. In addition, Fig. 4 shows the *HST* optical (*I*–*B*) colour image (using the original *HST* images, i.e. without any filtering process).

These figures show interesting structures, in particular the following.

(i) Bubble or shell – S1. This is the more external and well-defined supershell detected in Mrk 231, with a radius $R_{S1} = 3.5$ arcsec = 2.9 kpc. Lípari et al. (1994) have already noted that this shell shows a clear elongation to the south of the nucleus. At the border of this elongation, there is a blue arc with several knots. They associated this arc with typical structures generated in the blowout phase of a nuclear GW (with giant shocks). These shocks probably generated a new extranuclear star formation process, with knotty structure.

Fig. 2 shows interesting details of this superbubble + arc in the *HST* ACS, WFPC2 and NICMOS images. In particular, the *HST* WFPC2/*B* image depicts more clearly the shell S1. However, the *HST* ACS/*U* image shows remarkable details of the blue compact knots located at the border of the southern arc.

[1] IRAF is distributed by the National Optical Astronomy Observatories, which are operated by the Association of Universities for Research in Astronomy, Inc., under contract to the National Science Foundation.
[2] INTEGRAL is the imaging and spectroscopic analysis software facility developed by the Instituto de Astrofisica de Canarias (IAC).
[3] STSDAS is the reduction and analysis software facility developed by the Space Telescope Science Institute.
[4] SPECFIT was developed and is kindly provided by Gerard A. Kriss.
[5] ADHOC is a two-dimensional/three-dimensional kinematics analysis software developed by Marseille Observatory.

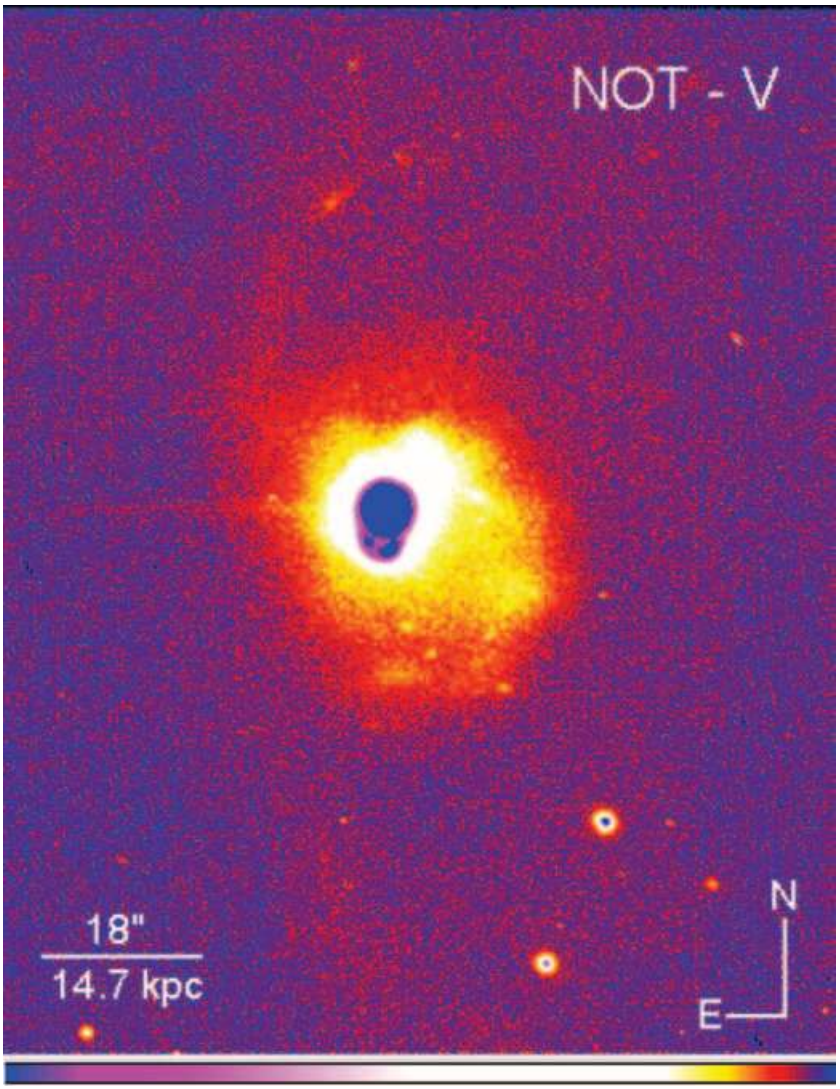

Figure 1. *V* broad-band image of the main body and the faint tails of Mrk 231 (obtained at the 2.5-m NOT telescope, La Palma, Spain).

(ii) Bubble – S2. The next internal superbubble/shell, at $R_{S2} = 1.8$ arcsec $= 1.5$ kpc, shows also a well-defined circular shape. However, this more internal bubble is clearly obscured in the south-east region (probably by reddening, associated with the presence of dust in the nuclear area). Again, the *HST* WFPC2/*B* image depicts more clearly the partial shell S2. It is important to remark that this shell shows a very interesting knot 2 in the south-west direction (see Table 3 and the next sections for details about the properties of this knot).

(iii) Shell – S3. The next superbubble, with a radius $R_{S3} = 1.2$ arcsec $= 1.0$ kpc, also depicts a circular shape, and its emission is strong mainly in the south area. This structure is well defined in the *HST* ACS/*U* image, which also shows a knotty structure. This shell depicts a bright knot 3, to the south-east.

(iv) Shell – S4. This shell is clearly observed mainly in the *HST* ACS/*U* image (see Fig. 2a; we note that this ACS image has the best spatial resolution) and also in the ACS/*U*, WFPC2/*B* residual images (Figs 3a and b). The radius of this shell S4 is $R_{S4} = 0.7$ arcsec $= 0.6$ kpc.

(v) Possible shell – S5. This possible shell is only observed in the *HST* optical (*I*–*B*) colour image (Fig. 4) and very close to the nucleus, with a radius $R_{S5} = 0.3$ arcsec $= 0.2$ kpc.

(vi) Close to the nucleus, the *HST* images show radial filaments. These structures are more clear in the near-IR image because at these wavelengths the dust absorption is significantly smaller. In particular, it has been found that these filaments are larger and clear in the direction north–south [position angle (PA) $\sim 00^{\circ}$] and at the PA of the radio jet (PA $\sim -115^{\circ}$; see Sections 4.2 and 4.3 for details about this jet). We note that these PAs are coincident with the directions of the two main OF processes in Mrk 231 (see the next sections). In our programme of study of GWs in IR mergers/QSOs, similar filaments were detected associated with the OF processes of NGC 3256, 2623 and 5514.

These types of circular and concentric 'superbubbles or shells' could be associated mainly with symmetric explosive events. In Sections 3.2 and 4.3 the kinematics, age, energy and possible origin of these structures will be discussed.

3.1.2 Circumnuclear knots

Table 3 presents the location and properties of the main knots, in the nuclear and circumnuclear areas of Mrk 231. In addition, the positions of these knots are labelled in Fig. 3b. Surace et al. (1998)

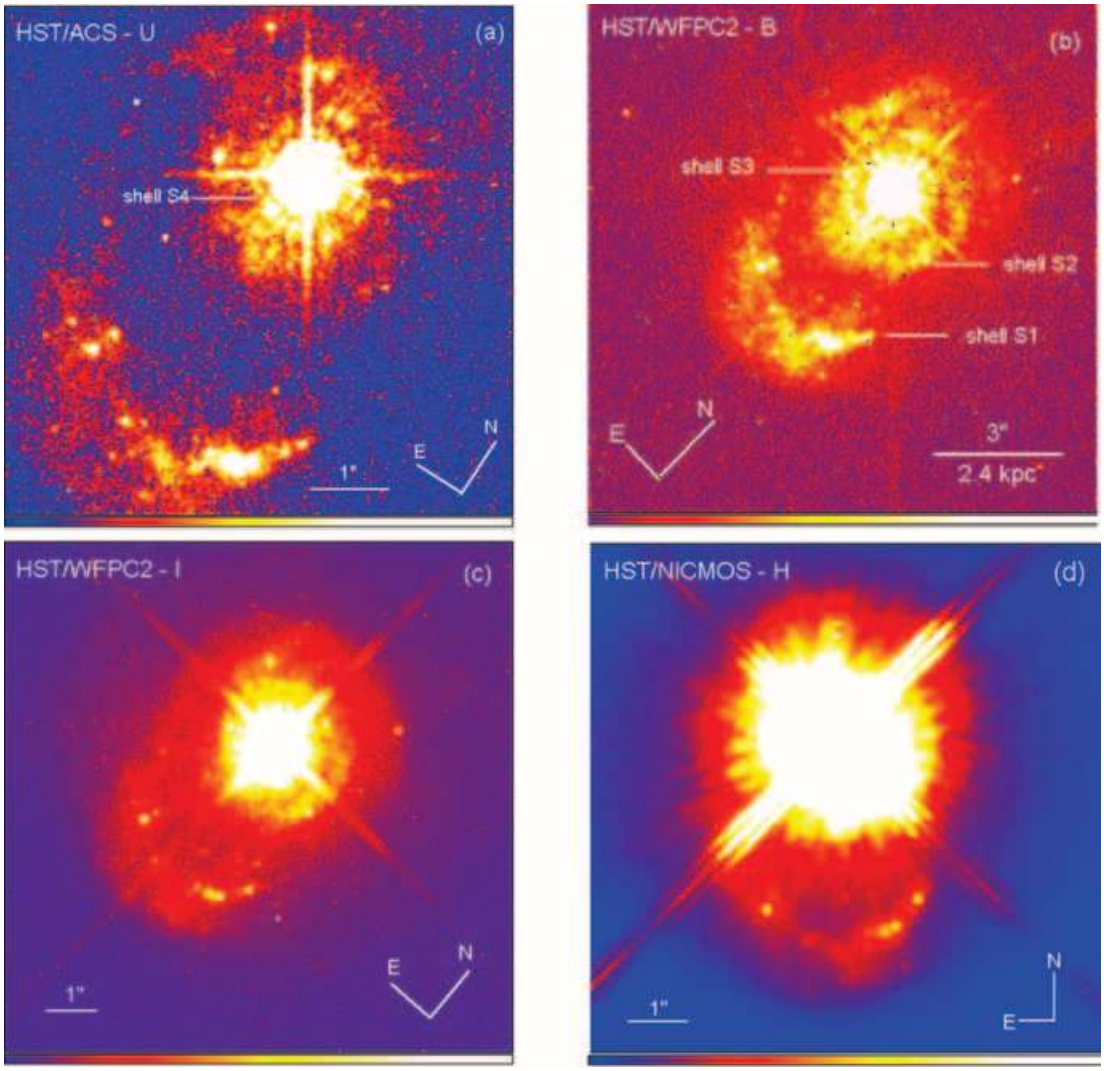

Figure 2. Near-UV, optical and near-IR *HST* broad-band images of the circumnuclear regions and the multiple concentric superbubbles/shells, in Mrk 231.

have already studied in detail these knots using *HST* photometry, in the *B* and *I* bands. In this paper, we study mainly their properties in relation to the process of OFs and their location in the shells.

From the data of Table 3, it is clear that in the southern part of the shell S1, the knots 5, 6, 11 and 12 show blue colours, probably associated with new star formation events. In particular, these knots emit a strong UV continuum, due to the presence of a large number of massive O and B stars. These massive stars are usually responsible for the rupture phase of the galactic bubble and are also the progenitors of core–collapse SNe. In the supergiant bubble of NGC 5514, we also detected the presence of several knots with massive Wolf–Rayet stars (inside the areas of rupture of the external shell). The radius of this bubble in NGC 5514 – just detected in the rupture phase – is also of ∼3 kpc, i.e. the same value of the supershell S1 in Mrk 231. We have already noted that the results of hydrodynamical models for GWs (associated mainly with extreme starbursts) suggest that 3 kpc is the typical value of radius for the beginning of the blowout phase (after ∼8 Myr, from the initial starburst; Suchkov et al. 1994).

The remaining knots show different colours (see Table 3). Some of the knots depict red colours, which could be explained – in part – by the presence of dust in star formation areas. In particular, the *HST* NICMOS image shows that knot 14 is bright at the *H* band, suggesting that the red colour in this knot (located in the southern arc of the supershell S1) is due mainly to reddening by dust. However, for the other two knots with very red colours, the 2D spectroscopy suggests another origin for the red colours. For knot 2 (located in the supershell S2) the spectrum shows properties typical of bow shocks, similar to those found in radio jets (for details, see the next section). In addition, knot 29 (positioned at the north-west area of the shell S1) also shows very red colour, and it is located in another OF region, where the [S II]/Hα and [N II]/Hα maps depict extended radial filament, probably emerging from the superbubble (see Section 3.4). For this area Krabbe et al. (1997) also reported OF ejection (of ∼1400 km s^{-1} in Paα; from a study of 2D near-IR spectroscopy).

In the next sections, the kinematics and physical properties of the multiple concentric supershells and the circumnuclear knots are analysed (using mainly WHT 2D spectroscopy).

3.2 Mapping the outflows in the nucleus and in the multiple supergiant bubbles (two-dimensional spectra)

The Hα+[N II] emission-line profiles obtained simultaneously with INTEGRAL for the central region of Mrk 231 (16 × 12 arcsec^2;

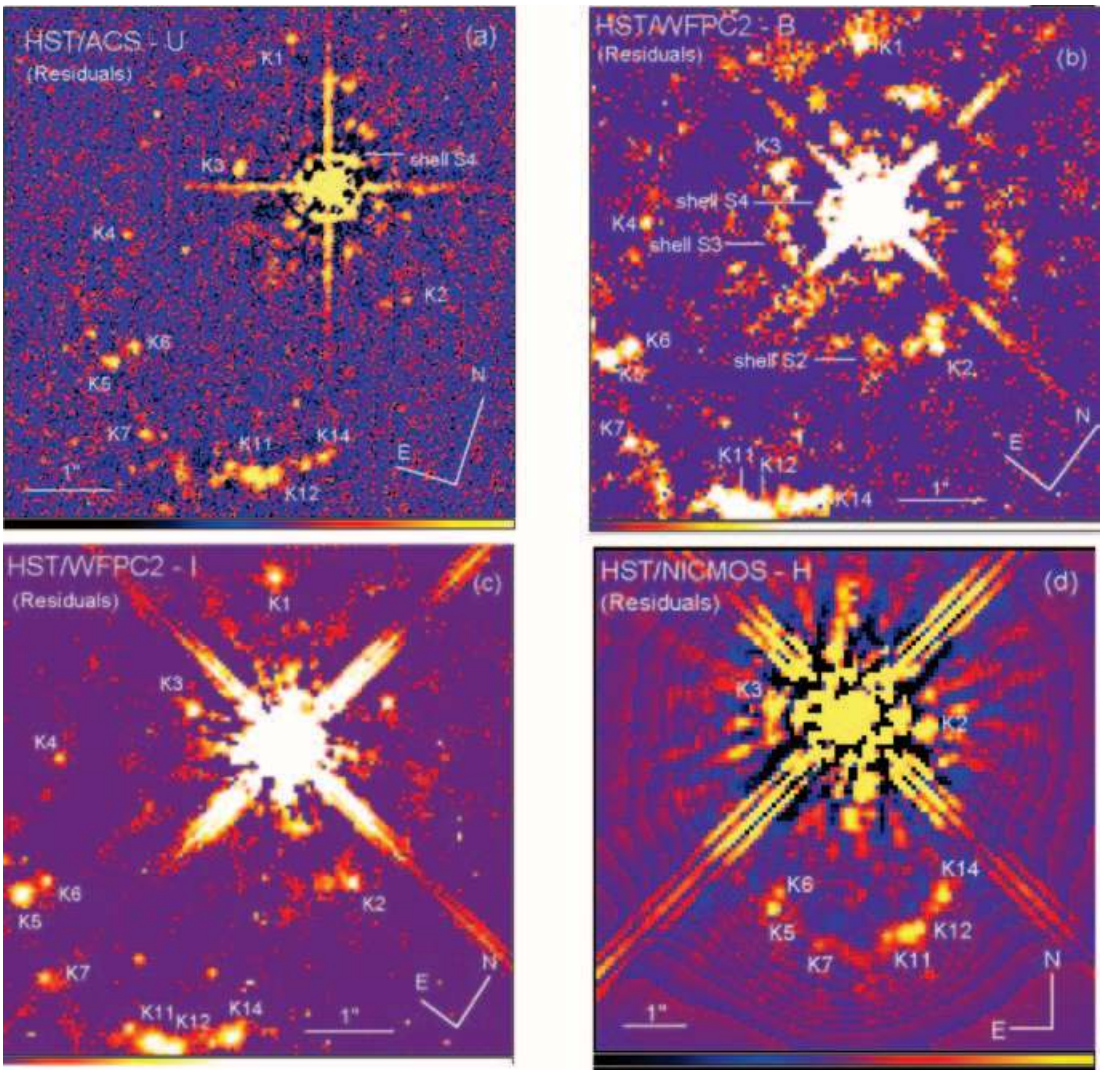

Figure 3. Near-UV, optical and near-IR *HST* broad-band residuals images of the circumnuclear region and multiple concentric supershells, in Mrk 231.

13.0 × 10.0 kpc^2) are shown in Fig. 5. These are reduced data, but represent only a small part (∼100 Å) of the full spectral coverage (6200–7600 Å) at each of the 189 fibre locations. The nucleus was positioned close to the centre of the field (at fibre 107), where the presence of broad emission lines is evident.

First, the OF at small scale will be analysed, in the region close to the nucleus (R < 1–2 kpc). In particular, it is important to note the following main results.

(i) In fibre 101 (adjacent to the fibre of the nucleus) the 2D spectrum shows the presence of an strong OF emission bump in the blend Hα+[N II], with the peak corresponding to the same velocity of the main BAL-I system ($V_{\rm Ejection\,BAL-I} \sim -4700$ km s^{-1}). More specifically, the Hα peak of this blue bump was measured using SPECFIT and SPLOT (for details, see Section 2), and a value of $\lambda = 6733$ Å was measured (corresponding to an ejection velocity of -4689 km s^{-1}).

This bump was detected in the area covered by this fibre, at 0.6–1.5 arcsec (490–1220 pc), to the south-west of the nucleus core at PA $\sim -120^\circ$, showing a strong and broad peak (see Fig. 6b).

It is important to note that the direction/PA of fibre 101 (from the main nucleus) is the same as the PA of the small-scale radio jet (PA$_{\rm jet} \sim -120^\circ$ to -110°).

(ii) Following the same direction (at PA $\sim -120^\circ$) in the next fibre (91; Fig. 6c) we found multiple narrow emission-line components, with a 'greatly' enhanced [N II]/Hα ratio, very similar to the spectra of jet bow shocks found in the Circinus galaxy (by Veilleux & Bland-Hawthorn 1997). This feature was detected at 1.7–2.5 arcsec (1340–2030 pc), inside the supershell S2 and coincident with knot 2.

The generation of a strong narrow-line region is expected from jet propagation in the ISM (Bicknell et al. 1998). We note that in the red border of the Hα bump, in fibre 101, we also detected the presence of multiple narrow emission-line components. None of the other fibres shows this type of strong narrow emission.

(iii) For the nucleus (i.e. fibre 107, r < 0.45 arcsec ∼366 pc) the blue OF bump was observed, but with relatively weak emission because it is superposed with the broad nuclear component (Fig. 6a).

In addition to this qualitative study of the blue Hα bump, we performed a detailed quantitative analysis for all the 2D spectra of the nuclear region, in a radius of r < 1 arcsec. It is important to note that in the blue side of the strong Hα bump (in fibre 101) we detected a relatively small emission component from the Fe II multiplet (74)λ6456; thus, it is important to study also the properties of the Fe II (74) emission. We measured the fluxes, equivalent width

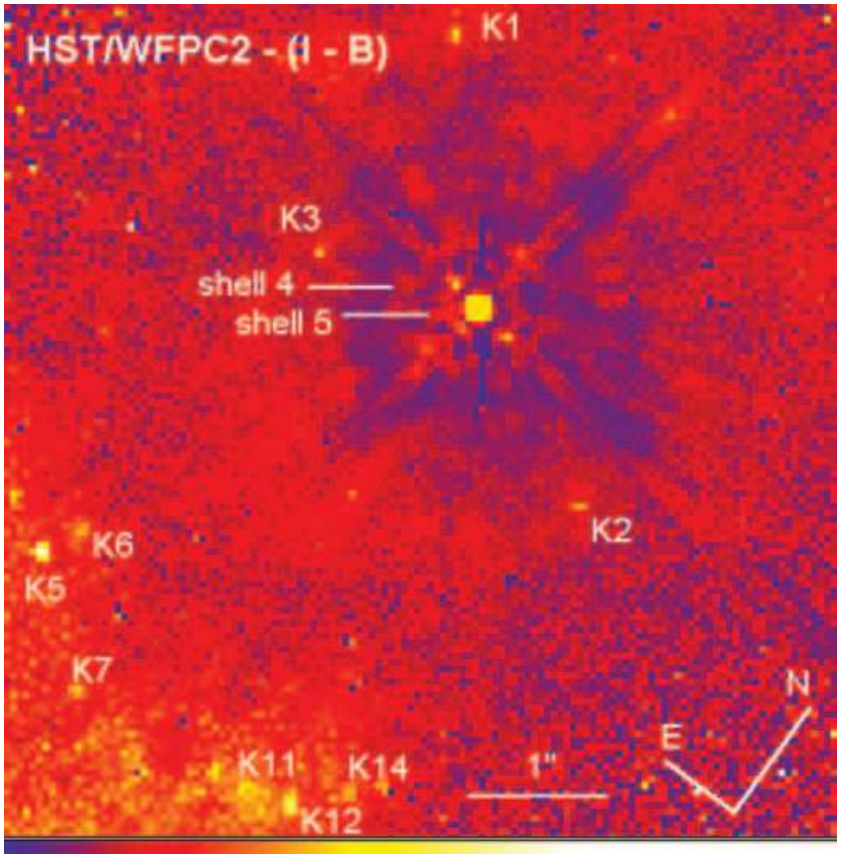

Figure 4. *HST* WFPC2 (*I*–*B*) colour images from the optical F814W and F439W filters.

Table 3. Main properties of the circumnuclear knots (associated with the supershells).

Knots[a]	$\Delta\alpha$[b] (arcsec)	$\Delta\delta$ (arcsec)	B_{F439W}[a] (mag)	I_{F814W}[a] (mag)	*B*–*I*	R_{eff}[a] (pc)	Shells
1	1.10	1.68	22.23	21.12	1.11	66	S1
2	−1.52	−0.90	23.27	20.86	2.41	<20	S2
3	1.10	−0.16	22.38	20.86	1.52	62	S3
4	2.12	−1.45	23.98	22.60	1.38	42	S1
5	1.70	−2.97	21.31	20.50	0.81	<20	S1
6	1.56	−2.74	22.97	22.28	0.69	71	S1
7	1.01	−3.70	22.69	21.47	1.22	38	S1
11	−0.46	−3.66	21.17	20.66	0.51	136	S1
12	−0.69	−3.61	21.46	20.70	0.76	31	S1
14	−1.20	−3.15	21.79	20.33	1.46	40	S1
29	−2.30	1.82	23.26	21.06	2.20	46	S1

Notes. [a]From Surace et al. (1998). [b]The offset positions of the knots [$\Delta\alpha$ (RA), $\Delta\delta$ (Dec.)] are given from the nucleus position (as 0,0).

(EqW) and emission-line width (FWHM) of the Hα bump and Fe II (74) emission lines, mainly for the 2D spectra/fibre of the very nucleus and for the six nearest fibres (located at a distance less than 1 arcsec from the nucleus, i.e. including fibre 101). Table 4 presents the results of this study. In particular, we note the following.

(i) At fibre 101, the Hα bump shows the strongest value of flux, of 12.7×10^{-15} erg cm^{-2} s^{-1}. In addition, this bump also shows a larger width, with FWHM of 2550 km s^{-1} [60 per cent larger that the typical FWHM of Fe II (74), of ∼1500 km s^{-1}]. Thus, these results are in agreement with the previous qualitative study, where fibre 101 depicts more clearly this Hα bump. These results show also that the Fe II contribution is – in FWHM – relatively small.

However, it is interesting to study in detail whether in this region the Fe II emission shows extended emission. In particular, it is important to analyse if the low-ionization broad-line region (BLR; including the Fe II, Mg II, O I emissions) could be closely associated with the radio jets (as suggested Norman & Miley 1984). Furthermore, it is important to study at subarcsecond scale the blue Hα bump, and the Na I D, Ca II H–K and He I BAL systems. Actually, Gemini GMOS Integral Field Spectroscopy observations are in progress (with high spectral and spatial resolution), in order to perform this study.

(ii) For the nucleus, the Hα bump also shows large values of flux and width. In particular, the FWHM of the bump is larger than those measured for the Fe II (74) emission.

(iii) At fibre 108 (with symmetric position – from the nucleus – than fibre 101 and at PA ∼ 60°), the Hα bump shows large values of FWHM, of 2480 km s^{-1}.

(iv) For the remaining fibres, the properties of the Hα bump (Table 4) suggest that they are associated mainly with the presence of nuclear Fe II (74) emission. We recall that the seeing for the INTEGRAL 2D spectra was ∼1 arcsec and these fibres were located very close to the nucleus (closer than ∼1 arcsec). Thus, the Fe II emission detected outside the very nucleus is due probably to the effect of the seeing.

These results are consistent with the interesting fact that the blue Hα bump (in fibres 101, 107 and possibly 108) and the BAL-I system could be related to OF clouds associated with the small-scale jet. A discussion of this point is presented in Section 4.3.

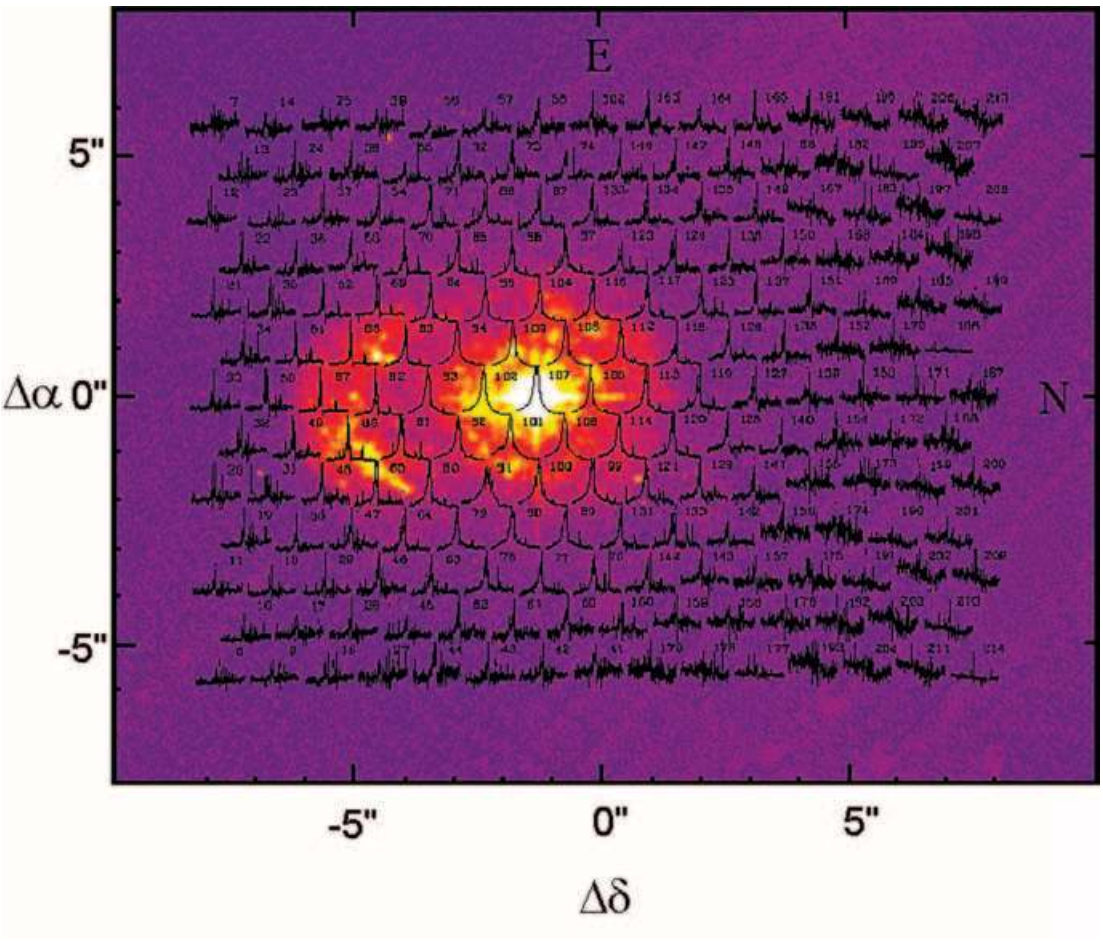

Figure 5. Superposition of the WHT + INTEGRAL 2D optical spectrum of the central region of Mrk 231 (for the Hα+[N II] blend) and the *HST* WFPC2/*B* image.

Now, the OF kinematics of the multiple supershells are analysed, for the central region ($R < 6$ kpc). In the three external superbubbles S1, S2 and S3, the 2D WHT spectra show multiple emission-line components (see Fig. 6), especially in the bright knots, where the following OF velocities values were measured.

(i) For the supershell S1:

(1) to the south, in knot 14 (fibre 065)

$\langle V_{\rm OF\,Shell-S1/South-F065}\rangle = [-420 \pm 30]$ km s^{-1};

(2) to the east, in knot 4 (fibre 084)

$\langle V_{\rm OF\,Shell-S1/East-F084}\rangle = [-485 \pm 30]$ km s^{-1};

(3) to the north-west, in knot 29 (fibre 131)

$\langle V_{\rm OF\,Shell-S1/North-West-F131}\rangle = [-500 \pm 30]$ km s^{-1};

(4) to the west, in fibre 077

$\langle V_{\rm OF\,Shell-S1/West-F077}\rangle = [-650 \pm 30]$ km s^{-1}.

(ii) For the supershell S2, in knot 2 (fibre 091)

$\langle V_{\rm OF\,Shell-S2/F091}\rangle = [-500 \pm 30]$ km s^{-1}.

(iii) For the supershell S3, in knot 3 (fibres 103, 102)

$\langle V_{\rm OF\,Shell-S3/F103}\rangle = [-230 \pm 40]$ km s^{-1}.

These values are consistent with expanding supergiant bubbles, and their properties and origin are discussed in Section 4.3

3.3 Velocity field of the ionized gas, in the nuclear and central regions (two-dimensional spectra)

In order to study the kinematics of the ionized gas, in the central region of Mrk 231, we measured the velocities from the centroids of the stronger emission lines Hα, [N II]λ6584 and [S II]$\lambda\lambda$6717–6731, fitting Gaussians (with the software SPLOT and SPECFIT; for details, see Section 2). In Mrk 231, first we studied the main emission-line component, which is strong in the whole of the central region. In the supershells the presence of multiple OF components required a detailed study.

Fig. 7 shows, for the ionized gas, the Hα velocity field (VF) for the central region $\sim$16 $\times$ 12 arcsec^2 $\sim$13 $\times$ 10 kpc^2, with a spatial resolution/sampling of 0.9 arcsec. This map was constructed using the techniques described in Section 2, and for the main component of the Hα emission lines. The errors vary from approximately $\pm$10 km s^{-1} in the nuclear and central regions (where the emission lines are strong), to $\sim$20 km s^{-1} for the weakest lines away from the nuclear areas. Using the 2D Hα VF, we have obtained a mean value of the systemic velocity $V_{\rm Syst} = 12\,645 \pm 10$ km s^{-1}; this value was defined as the zero of the VF.

The Hα isovelocity colour map (Fig. 7) shows interesting structures.

(i) Coincident with almost the border of the more extended superbubble or shell (S1), parts of a ring with blueshifted values of velocities and circular shape were detected. We note that this

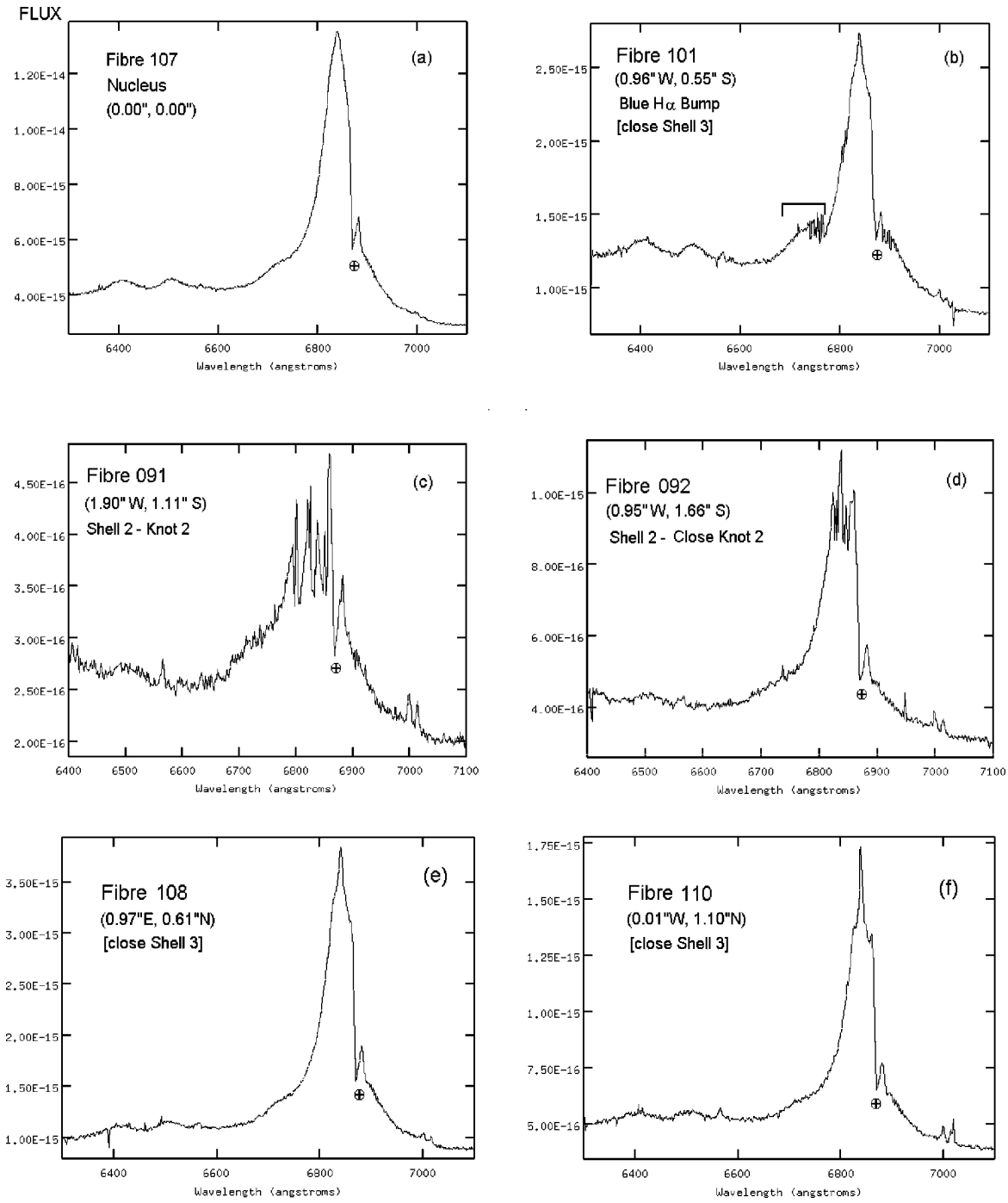

Figure 6. WHT + INTEGRAL 2D spectra (for individual fibres) in the main structures of the nuclear and circumnuclear regions of Mrk 231 (showing several OF components in the supershells). The scales of flux are given in units of erg cm^{-2} s^{-1} Å^{-1}.

structure reaches the south border of the field, and probably part of this ring (to the south) is located outside our INTEGRAL field. The radius of this structure/ring is $r \sim 5.0$ arcsec ~ 4 kpc.

(ii) Inside the ring, and close to the southern arc, two redshifted lobes were detected. Specifically, these structures are very close to the bright knots of the southern arc. Probably, these red lobes are associated with knots of rupture/blowout process (similar to those detected in NGC 5514; Lípari et al. 2004d).

In particular, in the region of the brightest knots K11 and K12 (in the southern arc), there is outside the shell/arc S1 a strong redshifted lobe, and inside S1 a weak blueshifted radial filament.

(iii) To the north-west, part of an elongated blueshifted lobe was found. In this structure we have measured high values of velocities of $\Delta V \sim -200$ km s^{-1}.

These results are clearly consistent with those found in Section 3.2. In particular, the detection of a blueshifted ring almost coincident with the position of the supershell S1 confirms the OF/expansion of this shell (even in the main component of the emission lines). The presence of an elongate blueshifted structure to the north-east (of the INTEGRAL VF) is also consistent with the detection – in this area – of filaments in the [S II]/Hα and [N II]/Hα maps (see

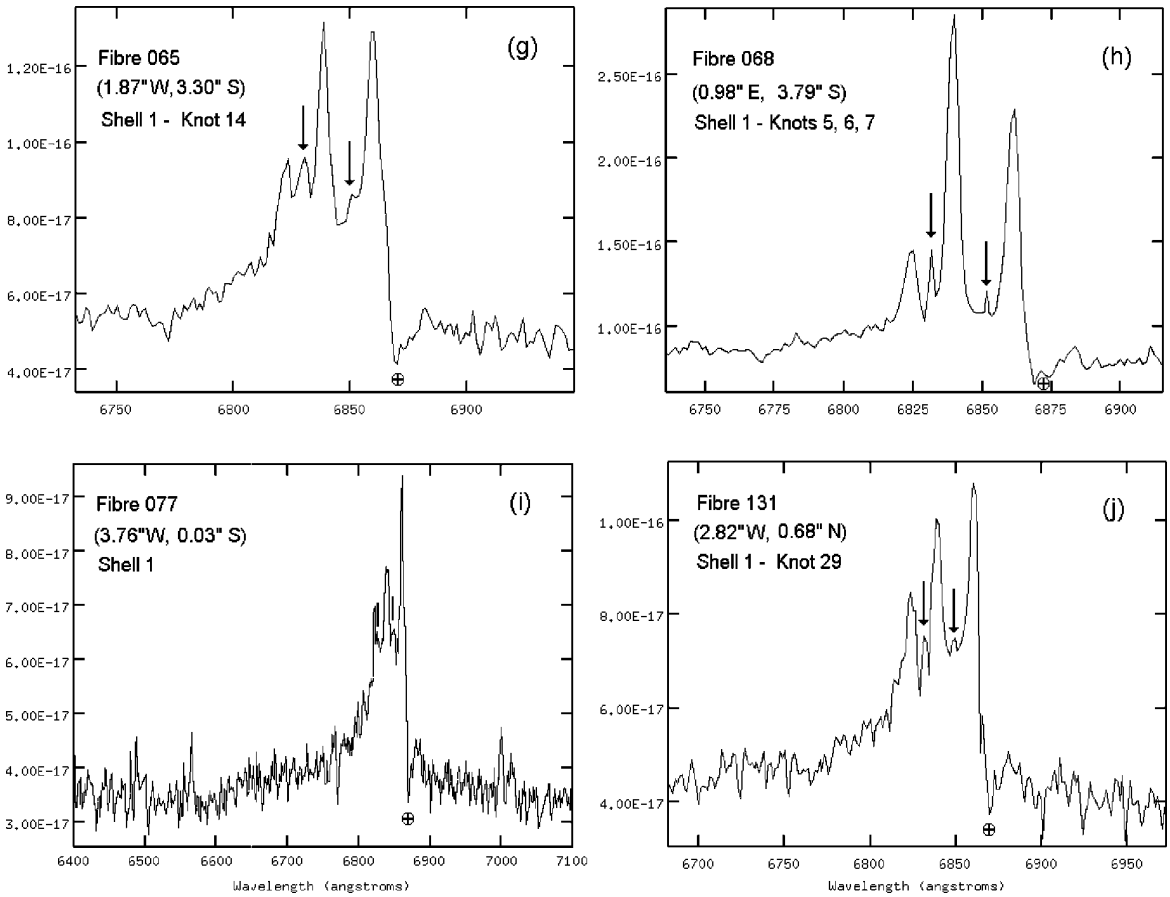

Figure 6 – *continued*

Table 4. Emission-line properties of the Hα bump and Fe II (74) (from WHT + INTEGRAL 2D spectroscopy).

Flux EqW/FWHM	Fibre 101 (1.0″ W, 0.6″ S)	Fibre 107 (0.0″, 0.0″)	Fibre 108 (1.0″ E, 0.6″ N)	Fibre 103 (1.0″ E, 0.5″ S)	Fibre 102 (0.0″, 1.1″ S)	Fibre 106 (1.0″ W, 0.6″ N)	Fibre 110 (0.0″, 1.1″ N)
Fluxes[a]							
Hα bump	12.7	8.9	3.6	1.2	2.8	2.1	–
Fe II (74)λ6148	6.9	16.1	4.5	8.2	7.9	2.4	2.0
Fe II(74)λ6248	4.9	17.5	4.0	7.2	7.0	2.1	3.0
Wavelength Peak (Å)							
λHα bump	6733	6730	6727	6725	6724	6723	–
EqW (Å)							
EqW Hα bump	6.8	2.5	2.2	4.0	2.3	3.3	–
EqW Fe II(74)λ6148	5.4	3.8	4.4	4.3	4.2	4.2	2.7
EqW Fe II(74)λ6248	4.0	4.1	4.0	3.1	3.1	3.8	4.3
FWHM (km s^{-1})							
FWHM Hα bump	2550	2300	2480	1730	1720	1880	–
FWHM Fe II(74)λ6148	1660	1620	1695	1760	1750	1700	1730
FWHM Fe II(74)λ6248	1550	1585	1690	1510	1600	1800	1740

Note. [a]The fluxes are given in units of 10^{-15} erg cm^{-2} s^{-1} (from 2D spectroscopy with a resolution of $\sim$100 km s^{-1}). The offsets are from the nucleus (at fibre 107).

Section 3.4) and the previous detection of an OF ejection (Krabbe et al. 1997).

3.4 Mapping the emission-line ratios and the ionization structure: large-scale galactic shocks

The set of 2D spectroscopic data, which cover the main structures of the central region of Mrk 231, allows the investigation of the ionization structure and the physical conditions in the gaseous phases. Figs 8(a) and (b) show 2D maps (of 16.4×12.3 arcsec^2, with 0.9 arcsec spatial sampling) of the emission-line ratios [N II]λ6583/Hα and [S II]λ6717 + 31/Hα. These maps were constructed using the techniques described in Section 2 and are based on the main component of the emission lines. Figs 8(c) and (d) show the values of these ratios for each fibre (which were used in the generation of the maps).

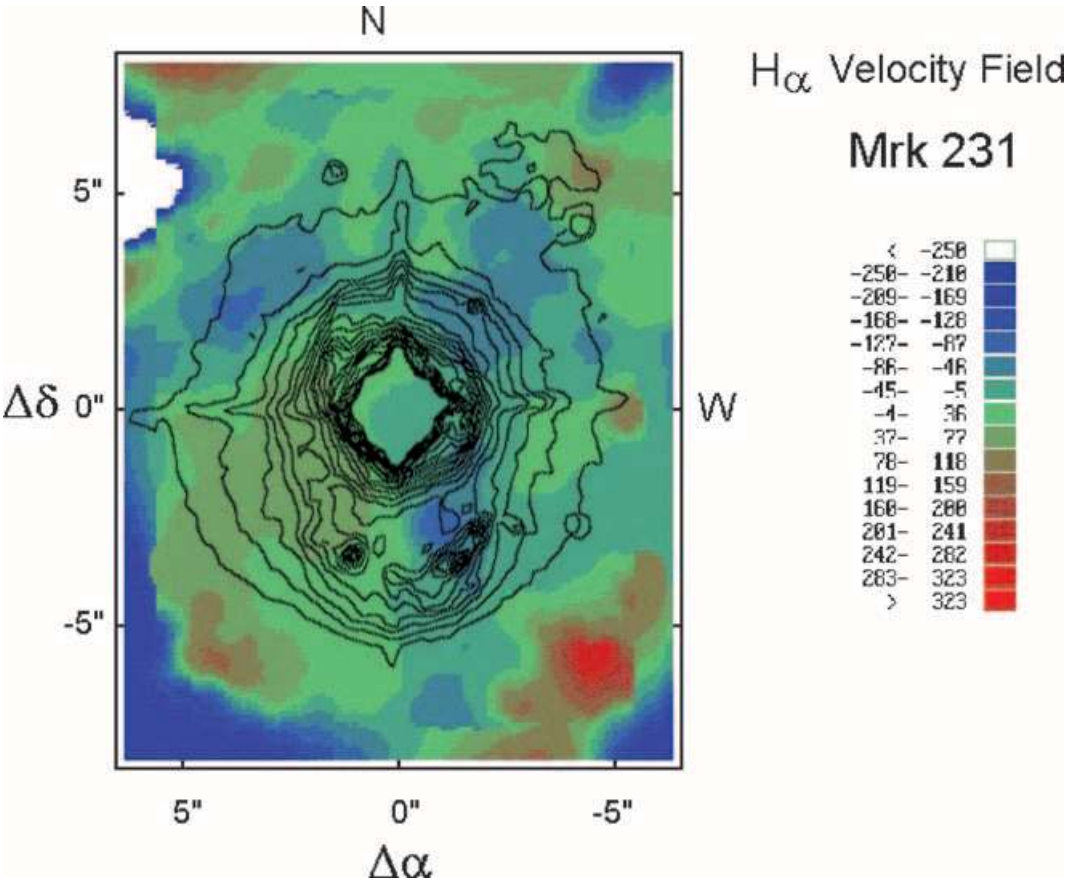

Figure 7. Superposition of the WHT + INTEGRAL kinematics map of the ionized gas (Hα, for the central region of Mrk 231) and the *HST* WFPC2/*I* contour.

Figs 8(a) and (b) show interesting features, and we note the following.

(i) For the area where we measured the narrow emission-line components, i.e. in almost all the circumnuclear region ($1.8 < r < 5$ arcsec; i.e. including the two more external supershells/bubbles S1 and S2), the [N II]/Hα emission-line ratios show high values (>0.8). This result, obtained from the 2D map (Fig. 8a) was verified using the individual spectrum of each fibre (Fig. 8c).

(ii) The [S II]λ6717 + 31/Hα map (Fig. 8b) also shows high values in the circumnuclear areas. In particular, we found a range of values for this ratio: $3 >$ [S II]λ6717 + 31/H$\alpha > 0.8$ (see Figs 8d and b).

(iii) Especially, to the north-west the [S II]λ6717 + 31/Hα and [N II]/Hα maps show filaments, which are probably associated with ejection from the superbubble. Lípari et al. (2004d) have already discussed in detail that the [S II]/Hα map is one of the best tracers of filaments associated with OF and shock processes.

Thus, in almost all the circumnuclear and central regions of Mrk 231 (including the supershells) these INTEGRAL emission-line ratio maps show high values (>0.8), which are consistent with an ionization process produced mainly by shock-heating in the outflowing gas of the expanding supergiant shells (Heckman 1980, 1996; Heckman, Armus & Miley 1987; Heckman et al. 1990; Dopita 1994; Dopita & Sutherland 1995; Lípari et al. 2004a,d). Furthermore, these ratios (for the main emission-line components) are located in the area of fast shock velocities of ~400–500 km s^{-1} in the upper part of the [N II]λ6583/Hα versus [S II]λ6717 + 31/Hα diagram (published by Dopita & Sutherland 1995, see their fig. 3a).

Similar results were obtained in the 2D studies of the superbubble NGC 3079 (Veilleux et al. 1994) and the OF nebula and superbubble of NGC 2623 and 5514 (Lípari et al. 2004a,d). They found that the ratios [N II]λ6583/Hα and [S II]λ6717 + 31/Hα are >1, in almost all the bubbles and the OF regions. They associated these results with the presence of large-scale OF + shocks.

3.5 Optical broad absorption line systems and the nuclear spectrum of Mrk 231 (one-dimensional spectra)

3.5.1 Optical broad absorption line systems: the variability of the Na I D BAL-III systems

It is important to study in detail the optical absorption and emission features of this IR QSO, in order to detect similarities and differences between this object and similar extreme IR + GW/OF + Fe II emitters. The optical and UV spectra of Mrk 231 (see Fig. 9a) present the features that are typical of extremely strong optical Fe II emitters with BALs (i.e. strong Na I D$\lambda\lambda$5889–5895 absorption, strong unresolved blends of optical Fe II lines, and very weak high-excitation forbidden emission lines). It is important to note the strong fall in the continuum flux at the UV wavelengths (this is also a typical feature of dusty luminous infrared galaxies; see Section 3.6).

Boksenberg et al. (1977) detected two non-stellar absorption-line systems (I and II) with velocities of 6250 and 8000 km s^{-1}, respectively. These correspond to ejection velocities of −6650 and −4950 km s^{-1}, with respect to the systemic velocity of 12 900 km s^{-1}.

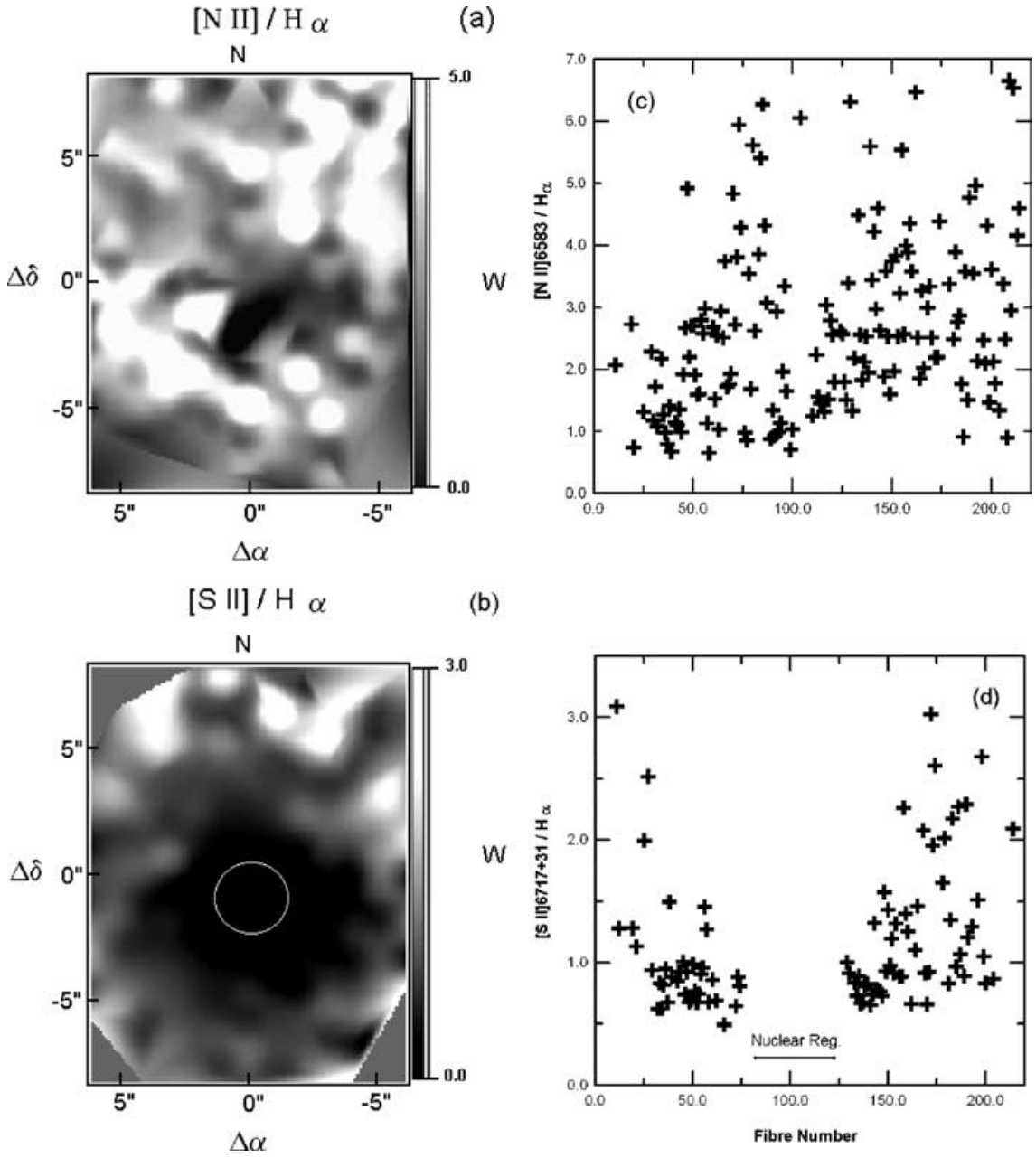

Figure 8. WHT + INTEGRAL maps of the emission-line ratios for the central region of the main body of Mrk 231. The circle in (b) shows the nuclear region, of Mrk 231 (in the field of WHT + INTEGRAL), where the narrow component of emission lines [S II] is very weak. (c) and (d) show the values of the emission-line ratios, for each individual fibre.

Boroson et al. (1991) detected a new absorption system III in the Na I D, Ca II H, K and He I, in their optical spectra of 1988. This system was not present in the spectra of Boksenberg et al. (1977), taken in 1975. With an observed radial velocity of 4660 km s^{-1}, this new system has the highest ejection velocity (-8240 km s^{-1}). The origin of these absorption-line systems has been discussed by Boroson et al. (1991), Kollatschny, Dietrich & Hagen (1992), Boroson & Meyers (1992), Lípari et al. (1994), Forster, Rich & McKarthy (1995), Smith et al. (1995), Rupke et al. (2002), and others.

It is interesting to recall the detection of another absorption system (IV), which corresponds to the systemic velocity and has a narrower absorption width. This system has already been associated by Boksenberg et al. (1977) with hot stars in the nucleus of Mrk 231.

Fig. 9(b) shows the BAL systems at the line Na I D. The corresponding width of these absorption systems are: FWHM of BAL systems I, II and III = 700, 130, 80 km s^{-1}, respectively. These are, in general, low values for BAL systems. Thus, these values are more consistent with those of mini-BALs or associated absorption lines (AALs; de Kool et al. 2001, 2002).

Now, we expand the previous study of variability of the Na I D BAL-III system (covering almost the whole period in which this system appeared). In order to study the behaviour of the variability of this absorption system, the measured values of the EqW ratio of BAL-III/(BAL-I + BAL-II) are included in Table 5. These data were obtained from our observation and also derived from published spectra (together with data previously published by Kollatschny et al. 1992 and Forster et al. 1995). We note that the previous study

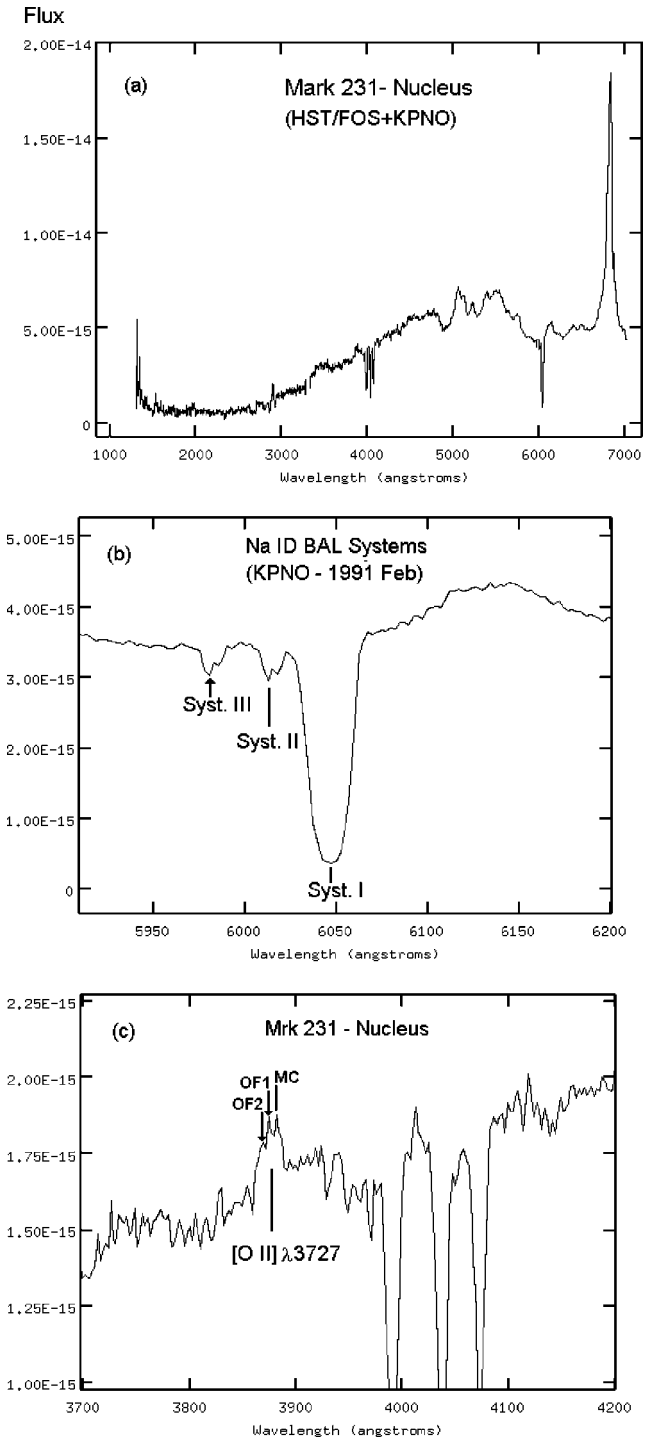

Figure 9. KPNO 1D optical spectra of Mrk 231. The scales of flux are given in units of erg cm^{-2} s^{-1} Å^{-1} and wavelength in Å.

of variability covers the period 1980–1992 (with only a few points after the maximum). The observations of Table 5 cover the period between ∼1980 and 2000. Figs 10(a) and (b) show the shape of the BAL-III light curve, which is clearly asymmetric with a steep increase, a clear maximum and an exponential fall. In particular, Fig. 10(b) shows a very good fit of the light curve fall, using an exponential function. In general, the shape of the BAL-III system light curve is similar to those light curves of SNe flux, emission line, etc.

Table 5. Relative variability of the Na I D BAL-III system.

Date	Julian Date 244 2507+	Intensity ratio	σ	References
Previous data				
1975/04/05	0000	0.000	0.000	(1) and (2)
1981/05/01	2218	<0.005	0.000	(1) and (3)
1984/12/21	3548	0.040	0.010	(1) and (4)
1987/02/02	4321	0.079	0.006	(1)
1988/07/06	4841	0.090	0.004	(5) and (1)
1992/01/10	6124	0.052	0.007	(1)
1992/05/21	6257	0.050	0.003	(1)
New data				
1991/02/01	5781	0.062	0.008	(6) and (7)
1991/02/15	5795	0.060	0.007	(6) and (8)
1994/04/22	6558	0.035	0.003	(6) and (9)
2001/02/28	9461	0.011	0.004	(6) and (10)

The references cited in column 5 are as follows: (1) Kollatschny et al. (1992); (2) Bocksenberg et al. (1977); (3) Hamilton & Keel (1987); (4) Schmidt & Miller (1985); (5) Boroson et al. (1991); (6) this paper; (7) Boroson & Meyers (1992); (8) Lípari et al. (1994); (9) Forster et al. (1995); (10) Rupke et al. (2002).

The probable origin of this BAL-III system is discussed in Section 4.3. Specifically, we discuss four possible scenarios. One of these scenarios is an explosive event associated with explosions of giant SNe/hypernovae (HyNe) – with very massive progenitors and located close to the AGN and/or in the accretion disc of the AGN.

It is important to note that previously it has been assumed that this light curve (of BAL-III) is symmetric. This type of variability was associated mainly with absorbing clouds crossing the central continuum light source (Kollatschny et al. 1992).

3.5.2 Outflow from the nuclear optical emission line

For the nuclear region of Mrk 231, a new detailed study of multiple emission-line components was performed. In particular, for the line [O II]λ3727 the presence of at least three components was detected (see Fig. 9c), with OF1 and OF2 velocities of −800 and −1300 km s^{-1}. The value of the OF previously reported by Lípari et al. (1994) was obtained from the blend of the OF1 + OF2. In addition, in the line Ni II an OF component was measured, with a value similar to OF1 (of [O II]).

It is interesting to note that Schmidt & Miller (1985), from a spectropolarimetry study, detected an OF velocity (for the dust) of −700 km s^{-1}. This is a value very close – within the errors – to our OF1 velocity.

A discussion of the extreme optical Fe II emission of this IR QSO was reported by Boksenberg et al. (1977) and Lípari et al. (1994). Ratios of Fe II$_{OPT}$/Hβ ∼ 8, [O III]5007/Hβ ∼ 0.01, Na I D/Hα ∼ 0.03 and Hα/Hβ ∼ 5 were measured. These results are in agreement with the typical values obtained for extreme Fe II$_{OPT}$ emitters, such as IRAS 07598+6508, PG 1700+518 and IRAS 18508−7815 (Lípari 1994).

3.6 Ultraviolet broad absorption line systems and spectrum of Mrk 231 and IR + GW/OF + Fe II quasi-stellar objects

3.6.1 Ultraviolet spectrum and broad absorption lines in Mrk 231

Significant reddening in luminous IR sources hampers the study of their UV properties. For Mrk 231, Figs 11(a), 11(b) and 9(a) show – at UV wavelengths – a strong reddening, with weak Mg II,

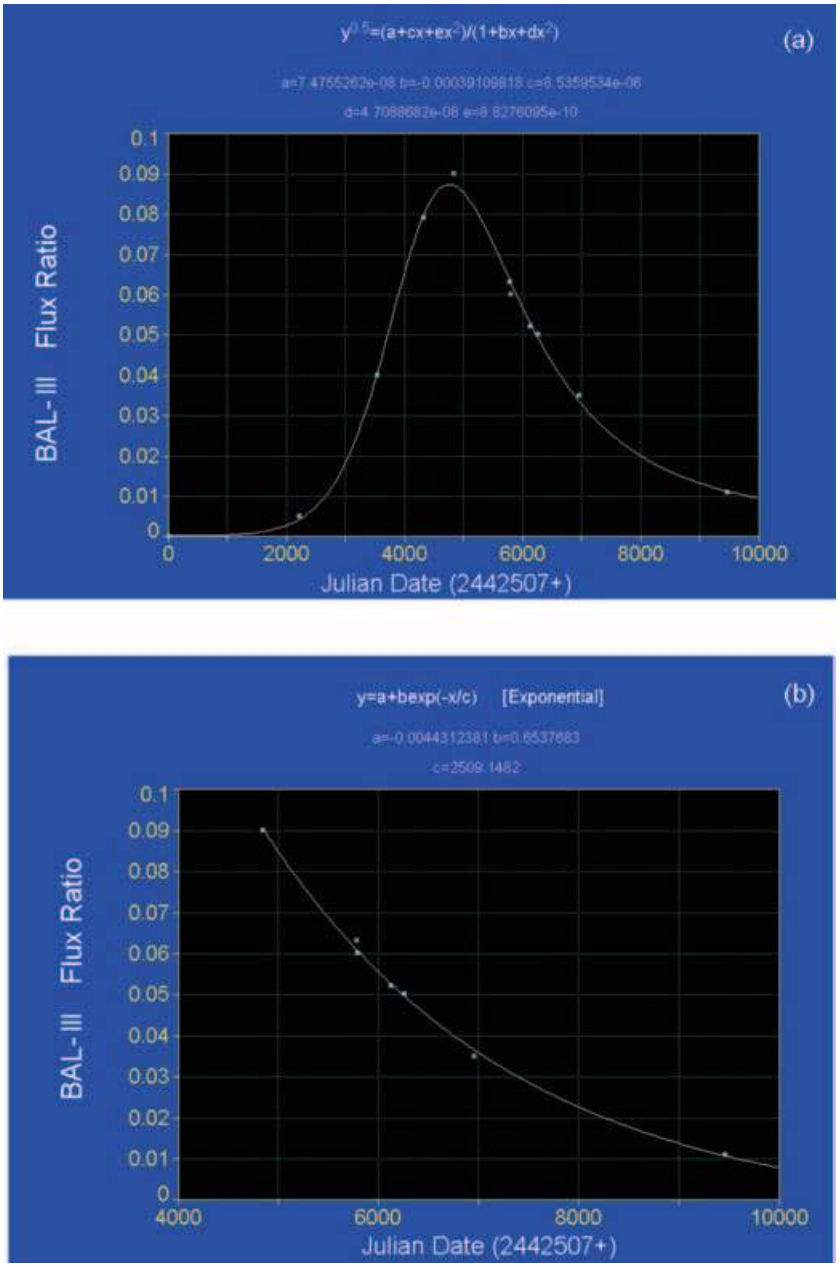

Figure 10. Light-curve variability of the Na I D BAL-III system, between the years 1975 and 2000 (a), and between 1988 and 2000 (b). The best fit of the light curve is also shown. For the fall of the light curve, the best fit is an exponential function.

C IV and Lyα emission lines. UV absorption associated with the BAL-I system are present in the Mg II and C IV lines (Figs 11a and b). In particular, the low-ionization emission-line Mg II is observed superposed to the BAL-I system (Fig. 11a). We measured for this absorption line a width (FWHM) of $\sim$700 km s^{-1}. This value is equal to that measured – in this system – in the Na I D optical line. In addition, in the region $\lambda\lambda$2000–2800 there are several absorptions due to UV Fe II.

It is important to study in detail the UV (plus optical) continuum of extreme IR–Fe II emitters and specifically BAL QSOs, because they show a clear deficit in the UV flux compared to the non-BAL QSOs (see Weymann et al. 1991; Sprayberry & Foltz 1992). Fig. 9(a) shows a clear drop in the level of the UV (and even in the *B*) continuum of Mrk 231, for λ shorter than 4500 Å.

3.6.2 Ultraviolet broad absorption lines in IR + GW/OF + Fe II quasi-stellar objects

From our programme of study and search of UV and optical BAL systems in extreme IR + GW/OF + Fe II QSOs, we have already found interesting results in relation to the UV low-ionization BAL system detected in IRAS 07598+6508 (Lípari 1994).

We recall that the standard definition of a BAL QSO (Weymann et al. 1991) is based on the measurement of the EqW of the C IVλ1549 resonance absorption-line system [called the balcity index (BI)]. QSOs with BI $>$ 0 km s^{-1} are considered BAL QSOs. In part for this reason, we observed the BAL candidates at UV (for C IV and Mg II lines) and optical (for Na I D absorption) wavelengths.

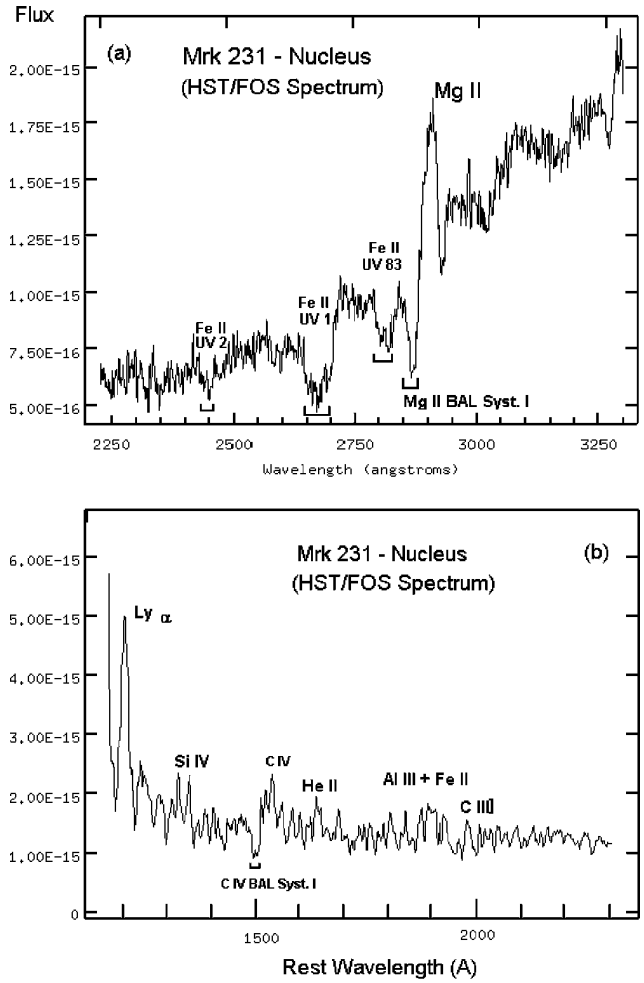

Figure 11. UV 1D *HST* FOS spectra of Mrk 231.

From this programme, the following main results were found.

(i) The UV–*IUE* spectrum of IRAS 21219−1757 (Figs 12a and b) clearly shows a blend of emission and absorption features – at low signal-to-noise – in the C IV line. In these two figures, the UV spectrum of IRAS 21219−1757 is superposed with the spectra of standard low-ionization BAL and non-BAL QSOs, respectively (obtained from Reichard et al. 2003). From these figures it is clear that the profile of the line C IV is very similar to the spectra of low-ionization BAL QSOs (and different to the spectra of non-BAL QSOs).

In general, the UV and optical spectral features of IRAS 21219−1757 are similar to those observed in nearby low-ionization BAL QSOs, such as IRAS 07598+6508 and PG 1700+518. These objects are also extreme IR + Fe II emitters (Lípari 1994; Wampler 1985; Lanzetta et al. 1993; Hines & Wills 1995).

In the *IUE*–UV (and optical) spectrum of IRAS 21219−1757 the following features were also observed.

(1) The absorption feature in the C IVλ1549 line extends from ∼1719 to ∼1665 Å, implying OF/ejection velocities of ∼1500 to ∼10 400 km s^{-1}.

The emission line of C IVλ1549 is also weak, as has been observed in BAL QSOs (Weymann et al. 1991).

(2) Figs 12(a) and (b) also show the presence of weak low- and high-ionization 'emission' lines. In particular, Lyα and N Vλ1240 are weak.

(3) There are also weak emissions from O Iλ1303 and Si IV + O IVλ1400.

(4) At optical wavelengths, in the blend Hα+[N II] we detected only one clear bump (which is not associated with Fe II emission) at λ = 7229 Å; corresponding to an OF velocity of −3373 km s^{-1}.

We note that the archive *HST*/STIS spectra of IRAS 21219−1757 do not cover the region where we detected the UV BAL in this IR QSO (the line C IVλ1549).

(ii) In order to compare this BAL IR QSO, with the previous observed BAL IR QSOs, we have also included in Fig. 13 the UV spectra of IRAS 07598+6508, PG 1700+518 and IRAS 14026+4341.

Furthermore, it is important to note that the UV BAL features observed in these IR + GW/OF + Fe II QSOs are very similar to those observed at high redshift in low-ionization BAL QSOs (at $z > 6.0$; see Maiolino et al. 2004a).

(iii) Fig. 13(d) presents the *IUE* spectrum of IRAS 18508−7815. In this extreme IR + GW/OF + Fe II QSO there is evidence of a possible/probable narrow absorption system in the line C IV (and close to the systemic velocity).

(iv) For PHL 1092 (another extreme IR + GW/OF + Fe II QSO) we have studied mainly the region of the Mg II + UV–Fe II emission line. Fig. 13(e) does not show evidence of Mg II BAL systems, in PHL 1092. However, the fit of the emission line in this area required to include an UV Fe II template (we used the UV Fe II emission of I Zw 1, from the *HST* spectra) and also a blue OF component. For this blue component, an OF value of −8565 km s^{-1} was measured.

At optical/red wavelengths, this OF (with very high velocity) was not detected at the line Hα. However, we found three blue OF components with relatively low velocities. For these blue components, the following OF values were measured: OF1 = −1500, OF2 = −2500 and OF3 = −3100 km s^{-1} (see Fig. 13f). These velocities are almost the same as those obtained for the OFs detected in Hβ (using the offset method; Lípari et al. 2004d, see their table 8).

It is important to note that Dietrich et al. (2002) and Barth et al. (2003) have already discussed that in order to obtain a good fit of the UV emission lines Mg II + Fe II in very high-redshift QSOs, they need to include a strong blueshifted component (they explain that this component was used without a physical explanation). In particular, Barth et al. (2003) in their fig. 2 show this strong blue OF component in the line Mg II, for the Fe II QSO SDSS J114816.64+525150.3. This object is one of the younger QSOs known, with a redshift $z = 6.4$. They measured for the Mg II OF component – of this distant/young QSO – a value of ∼ −5700 km s^{-1} (Barth et al. 2003, see their fig. 2), which is almost one-third smaller than the value obtained for PHL 1092.

Therefore, we strongly suggest that this type of blue component observed in the Mg II emission line – in very high-redshift QSOs – is associated with extreme OF processes. Again, the results obtained from QSOs at very high redshift (by Dietrich et al. 2002 and Barth et al. 2003) are very similar to our results for IR + GW + Fe II QSOs at low redshift (where we detected blue OF components in Hα, Hβ, [O III], [O II] and Mg II emission lines). However, these OF emissions are probably associated with very different OF processes, similar to those found in this paper for Mrk 231.

4 DISCUSSION

In this section we discuss the properties of Mrk 231 as: (i) an evolving elliptical galaxy; (ii) a merger with composite nuclear energy; (iii) an EVOF QSO, with also a composite nature; (iv) as an exploding QSO. In addition, we analyse the IR colour diagram for a large

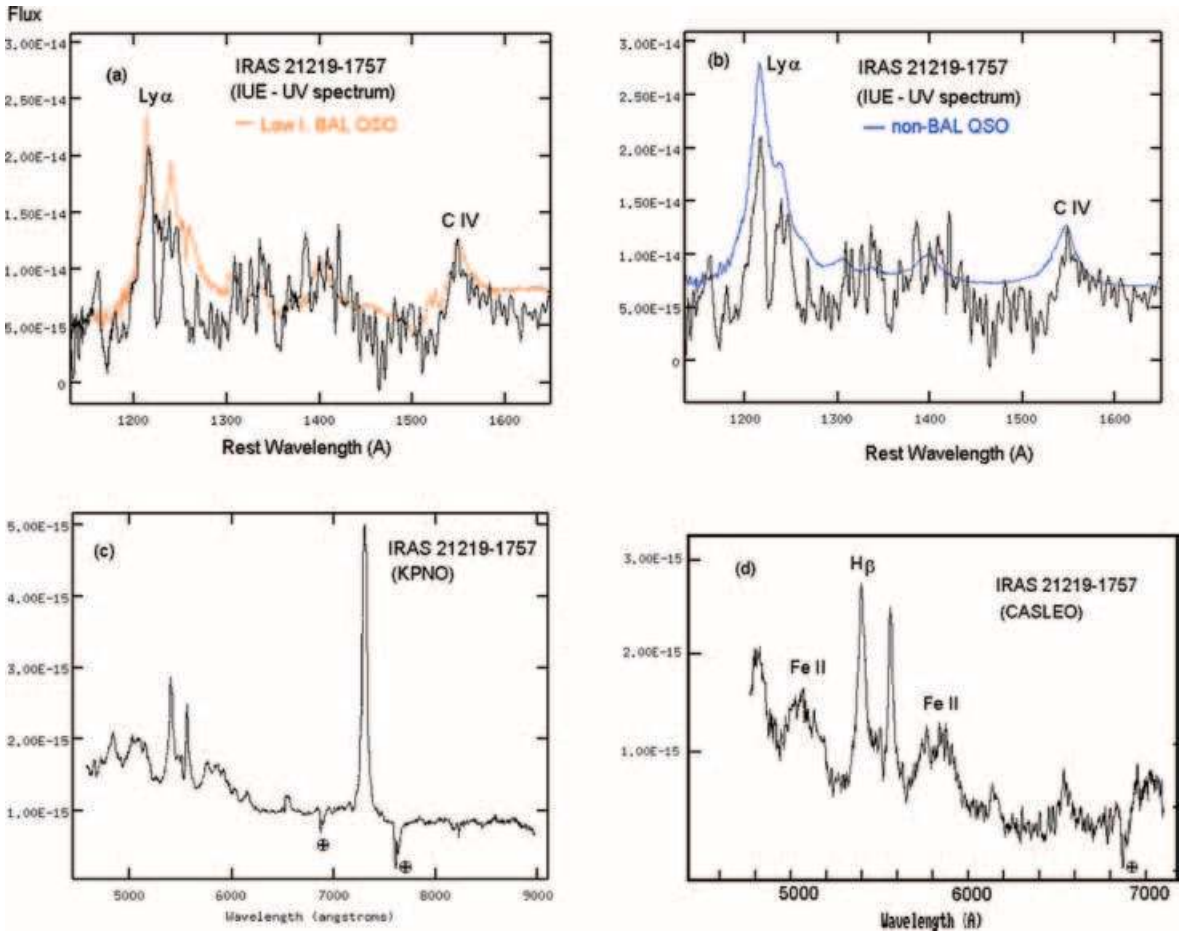

Figure 12. UV and optical spectra of the IR + GW/OF + Fe II QSO IRAS 21219−1757 showing UV BAL systems.

sample of IR mergers/QSOs with GWs (including BAL QSOs and Mrk 231).

4.1 The merger Mrk 231 as an evolving elliptical galaxy with galactic wind

Hamilton & Keel (1987) have already found that the optical *R* broad-band surface brightness profiles of Mrk 231 follow the $r^{1/4}$ law (in the range $1.0 \leqslant r \leqslant 10$ kpc). From high-resolution NOT *V* broad-band images, Lípari et al. (1994) found that the nucleus is compact at scales of 0.7 arcsec (∼500 pc). Using Keck mid-IR 7.9–19.7 μm broad-band images, Soifer et al. (2000) found that the nucleus is compact and unresolved at 0.13 arcsec (100 pc). At radio wavelengths, Condon et al. (1991) also detected an unresolved radio core, smaller than 0.25 arcsec (at 8.44 GHz), in Mrk 231. *HST* ACS/*U*, WFPC2/*I* and NICMOS/*H* broad-band images (see Section 3 and Quillen et al. 2001) confirmed that at scales better than 0.1 arcsec (∼80 pc, FWHM), the bright compact nuclear peak is unresolved. These results suggest that the nuclei of the original colliding galaxies have coalesced into a common nucleus with an AGN, and that the merger is in a very advanced phase (a relaxed system), probably evolving into an elliptical galaxy.

Therefore, Mrk 231 is another candidate for a proto-elliptical galaxy. It is important to note that from the theoretical point of view there is a wealth of literature proposing a relevant role for GW and OF in the formation and evolution of elliptical galaxies. We can highlight the following. (i) Mathews & Baker (1971) suggested that a GW can explain the deficiency of observed gas compared to that returned by stars in ellipticals. (ii) Larson (1974), Vader (1986) and Kauffmann & Charlot (1998) proposed for ellipticals a GW associated with the early star formation episode to explain their colour–magnitude and mass–metallicity relations. (iii) Larson (1974), Vader (1987) and Dekel & Silk (1986) proposed that dwarf ellipticals evolved from initially more massive elliptical galaxies that suffered substantial gas loss through SN-driven GWs. (iv) Scannapieco et al. (2001) studying the effect of galaxy OFs in the formation of dwarf galaxies found in the OF a natural explanation for the formation of empty haloes.

The results obtained for Mrk 231 (and previous studies of mergers with OF) suggest that extreme starbursts plus AGNs with GWs play an important role in galaxy evolution, e.g. giant expanding shells in composite GWs could produce BAL systems, massive starbursts could generate AGNs/QSOs, successive extreme starburst processes could transform the observed high gas density (in the ISM of mergers) to high stellar density, etc. Furthermore, these extreme–starburst + AGNs with GWs – induced by mergers – could be a nearby analogy for processes that occurred at high redshift, when the galaxies and QSOs formed, i.e. similar to the first massive star formation episodes (Population III stars) in hierarchical mergers and/or primordial collapses (Larson 1998, 1999, 2003; Bromm, Coppi & Larson 1999; Scannapieco & Broadhurst 2001; Bromm & Loeb 2003).

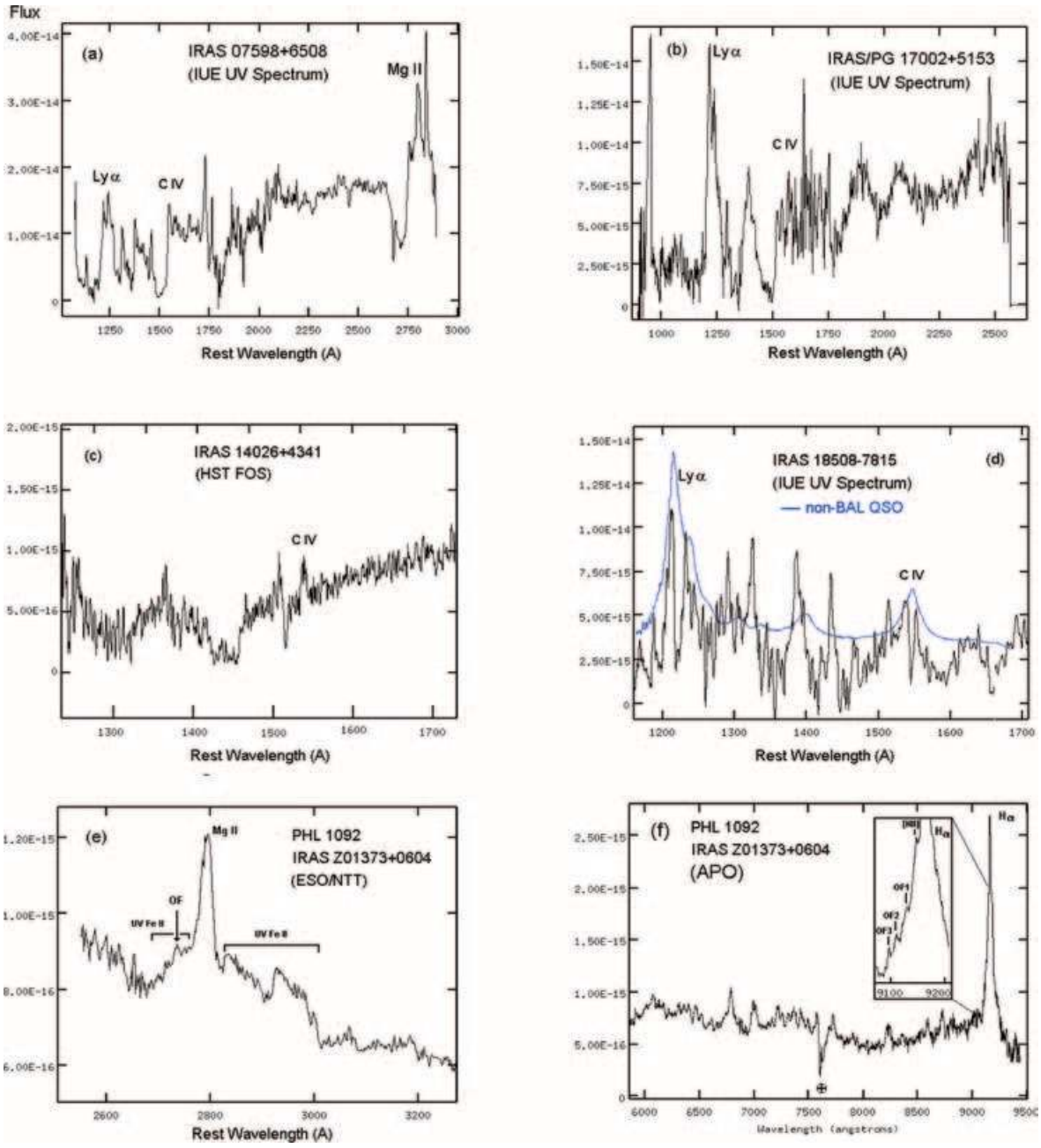

Figure 13. UV and optical spectra of IR + GW/OF + Fe II QSOs (including specially the BAL IR QSOs).

4.2 The composite nucleus of Mrk 231: an active galactic nucleus/quasi-stellar object embedded in an extreme starburst

In order to study the nature and origin of the complex nuclear OF process detected in Mrk 231, it is important to analyse the composite nature of the nuclear energy.

4.2.1 Active galactic nucleus/quasi-stellar object

There is clear and interesting evidence of the presence of an AGN/QSO in the nucleus of Mrk 231. Specifically, at radio wavelength Preuss & Fosbury (1983) have already detected a very compact nuclear radio source, at scale <1 pc (using very long baseline interferometry observations). Recently, using the Very Long Baseline Array (VLBA), Ulvestad, Wrobel & Carilli (1999a) and Ulvestad et al. (1999b) found a parsec-scale radio jet, with an extension of $\sim$2.5 pc.

At X-ray wavelength, using *ASCA* data, Turner (1999) has found that the optical-to-X-ray spectrum of Mrk 231 is typical of a QSO. In addition, using *Chandra* observations, Gallagher et al. (2002) have detected that the bulk of the X-ray luminosity is emitted from an unresolved nuclear point source and the spectrum is remarkably hard.

In Section 3, we found clear evidence that – at least – the Na I D BAL-I system is associated with the presence of the AGN + jet.

4.2.2 Extreme starburst

Recently, the star formation in the nucleus of Mrk 231 was studied at very high resolution by Bryant & Scoville (1996), Downes

& Solomon (1998) and Davies, Tacconi & Genzel (2004). In particular, Bryant & Scoville (1996) found that the CO distribution is elongated with kinematics properties consistent with a disc oriented in the east–west direction, and containing a mass of 3×10^9 $M_\odot$ of molecular gas (within a diameter of 1.0 arcsec, 814 pc). Downes & Solomon (1998) using CO interferometer data also detected a 1.2-arcsec diameter inner disc plus a 3.0-arcsec diameter outer disc. They found extreme star formation processes in the nuclear CO discs or rings of Mrk 231. These results confirm – at high resolution – previous studies that already suggested the presence of a strong nuclear starburst in this IR merger (Hamilton & Keel 1987; Hutching & Neff 1987, and others). In particular, Lípari et al. (1994) also suggested the presence of an extreme nuclear starburst, as the main source of the strong GW, detected in Mrk 231. These works suggest that at least one-third of the total source of the nuclear energy in Mrk 231 is generated by the extreme starburst.

On the other hand, continuum observations at 21 cm with the VLBA (Carilli, Wrobel & Ulvestad 1998) show emission from an extended disc of 370 pc, which exhibits absorption against the radio emission from the inner disc ($r < 160$ pc). Further radio continuum observations reported by Taylor et al. (1999) trace this emission out to 1.0 arcsec. They interpret this disc radio emission also as due to strong star formation activity with a star formation rate of 60–200 $M_\odot$ yr^{-1}. At near-IR wavelengths, the nuclear spectrum of this galaxy shows an anomalously large Paα/Brγ ratio (Cutri et al. 1984), which implies that the electron density in the broad-line clouds of Mrk 231 is higher than the standard values of the BLR in AGNs/QSOs.

In Section 3.4, it was found that extended shocks (associated with multiple expanding superbubbles) are also an important source of energy and ionization, in the nuclear and circumnuclear regions. In addition, we found evidence of a multiple explosive event in Mrk 231, which is in part associated with the extreme starburst, probably generated during the merger process.

Thus, at least two strong starbursts were generated in the merger process of Mrk 231: one associated with the origin of an extended post-starburst population (associated with the underlying hot stellar population in the optical spectrum), plus a young and dusty nuclear extreme starburst.

4.3 The composite nuclear outflow + BAL systems in Mrk 231: an exploding QSO?

In Section 3 we found very interesting results, about the OF and BAL systems in Mrk 231. Specifically, we detected: (i) multiple concentric expanding superbubbles; (ii) a blue Hα emission bump at the ejection velocity of BAL-I; (iii) a light curve for the BAL-III system showing a steep increase and exponential fall (very similar to the shape of an SN light curve).

In order to analyse these new results, it is important to note previous studies at radio wavelengths, which are relevant for the discussion of the OF in Mrk 231, in particular the following.

(i) Very long baseline interferometry images at 1.7 Ghz (Neff & Ulvestad 1988; Lonsdale et al. 2003) and VLBA images at 2.3 Ghz (Ulvestad et al. 1999a) show a north–south triple structure with a central unresolved core and two symmetric resolved lobes, with a total extension of ∼40 pc. This radio structure is elongated (at PA $\sim 00^\circ$) in the direction perpendicular to a 350-pc HI + CO starburst disc/ring.

(ii) Very Large Array images at 4.9 Ghz (Baum et al. 1993) and at 1.5 Ghz (Ulvestad et al. 1999a) show a very large structure of ∼35–50 kpc, also elongated in the north–south direction.

(iii) Using the VLBA at 15.3 GHz, Ulvestad et al. (1999a,b) found a parsec-scale radio jet, with an extension of ∼2.5 pc, low apparent speed, and at PA $\sim -115^\circ$.

4.3.1 Multiple expanding supershells

The presence of multiple concentric expanding supergiant bubbles/shells, with the centre in the nucleus and with highly symmetric circular shape could be associated mainly with giant symmetric explosive events. These giant explosive events could be explained in a composite scenario: where mainly the interaction between the starburst and the AGN could generate giant explosive events. In particular, Artymowicz, Lin & Wampler (1993) and Collin & Zahn (1999) have already analysed the evolution of the star formation close to SMBHs and inside accretion discs. They have suggested that the condition of the star formation close to the AGNs could be similar to those of the early/first star formation events, where giant explosive processes are expected, generated by HyNe (with very massive progenitors, $M \sim 100$–200 $M_\odot$; see Heger & Woosley 2002; Heger et al. 2002, 2003). In accretion discs, the star–gas interactions can lead to a special mode of massive star formation. Furthermore, the residuals of the first SNe (neutron stars) can undergo a new accretion/interaction phase, with the gas, leading to very powerful SN or HyN explosions.

For the supershell S1, Lípari et al. (1994) already proposed that the morphology and kinematics of the blue arc (located to the south of the nucleus) are in agreement with the results of GWs from hydrodynamic models. Specifically, the starburst GW models of Suchkov et al. (1994) predict after 8 Myr in the blowout phase: blue arcs with radius $r \sim 3$ kpc. We noted that after 8 Myr the starburst is in the Type II SN phase.

It is important to remark that exactly in the direction of this arc (north–south from the nucleus, PA $\sim 00^\circ$), Neff & Ulvestad (1988) and Ulvestad et al. (1999a) found an elongated structure of ∼40 pc, which is perpendicular to the CO starburst disc/ring. Furthermore, Baum et al. (1993) and Ulvestad et al. (1999a) detected a large structure (of ∼35–50 kpc), also elongated in the north–south direction. These results are all clearly consistent with the blowout or rupture phase of the superbubble S1.

Following our study of the superbubble in NGC 5514 (Lípari et al. 2004d), the dynamical time-scale of the more extended supershells S1 and S2 in Mrk 231 were derived, using the relation

$$t_{\rm dyn} = 1.0 \times 10^6 \; R_{\rm bubble,\,kpc} \; V^{-1}_{\rm bubble,\,1000} \; {\rm yr},$$

where $R_{\rm bubble,\,kpc}$ and $V^{-1}{}_{\rm bubble,\,1000}$ are the linear dimension of the bubble and the velocity of the entrained material (in units of kpc and 1000 km s^{-1}, respectively). The following values were obtained for the shells S1 and S2:

$$t_{\rm dyn-S1} \sim 4.8 \times 10^6 \; {\rm yr}; \qquad t_{\rm dyn-S2} \sim 3.0 \times 10^6 \; {\rm yr}.$$

Then a period of $\sim 2 \times 10^6$ yr is the separation between the two explosive events that probably generated the supershells S1 and S2.

From the 2D spectra, a mean value of Hα flux of 0.5×10^{-13} erg cm^{-2} s^{-1} was obtained, for the OF associated with the supershell S1. Using the relations given by Mendes de Oliveira et al. (1998) and Colina, Lípari & Macchetto (1991) a value for the ionized-gas mass, in the OF associated with the supershell S1, of 2.0×10^6 $M_\odot$ was found. Using this value of ionized-gas mass, we derived

for the kinetic energy of the OF–S1, $E_{\rm KIN\,OF-S1} \sim 0.5 \times M_{\rm OF-IG} \times \langle V_{\rm OF-S1}\rangle^2 = 2.0 \times 10^{54}$ erg. This high level of energy obviously required the presence of multiple SN events, or an unusual type of 'giant SN' or HyNe. Heiles (1979) has already suggested that this last alternative needs to be considered seriously, in order to explain supershells with energy $>3.0 \times 10^{52}$ erg (even if these energies of supershells are hundreds of times larger than that available from a single and 'standard' SN). In Section 4.3.4, we discuss the origin of the multiple supershells, mainly in the framework of an exploding HyN scenario.

4.3.2 Blue Hα emission bump at velocity of BAL-I system

In Section 3 another interesting results was found: a blue Hα emission bump at the ejection velocity of BAL-I (and in an area located very close to the nucleus and at the same PA as the radio jet). Furthermore, in the same direction where we detected this bump (at PA $\sim -120^\circ$ to -110°) at 1.3–2.2 arcsec, we also found multiple narrow emission-line components, with a 'greatly' enhanced [N II]/Hα ratio (very similar to the spectra of jet bow shocks). These results are consistent with a scenario where the BAL-I system is generated in OF clouds associated with the parsec-scale jet.

It is important to note that de Kool et al. (2001, 2002) found a very interesting result – and physically similar to those found for Mrk 231 – in their Keck high-resolution spectroscopic study of AALs and BALs, in the QSOs FIRST J104459.6+365605 and FBQS 0840+3633. The absorption lines of these QSOs cover velocity ranges of -200 to -1200 and -3400 to -5200 km s^{-1}, and the width of the individual absorption lines ranges from 50 to 1000 km s^{-1} (these are values similar to those measured in Mrk 231). They found that the distances between the AGN and the region where the OF gas generates the AALs and BALs are ∼700 and ∼230 pc, respectively. Therefore, for Mrk 231 (BAL-I system), J104459.6+365605 and FBQS 0840+3633, the distances found between BAL- or AAL-forming regions and the continuum source (AGN) are large, ∼200–1000 pc (BALs and AALs are generally thought to be formed in OFs at a much smaller distance from the nucleus; de Kool et al. 2001).

From a theoretical point of view, two main scenarios were proposed in order to explain BAL systems in AGNs/QSOs. (i) In outflowing equatorial wind models, the BALs are described in terms of a line-driven wind manifested as a skin flowing above a black hole accretion disc. This equatorial wind driven from the luminous disc is viewed at low latitudes, just above the molecular gas (for details, see Murray et al. 1995; Proga, Stone & Kallman 2000). (ii) In bipolar jet wind models, the BALs are associated with thin absorbing clouds in the OF of small-scale jets of AGNs (Punsly 1999a,b). Specifically, in the non-magnetic vortex of an accretion flow around an SMBH (i.e. radio-quiet QSO) only very weak and subrelativistic radio jets can be formed. These are radiation pressure-driven hypersonic jets, which can generate collimated bipolar OF. Punsly & Lípari (2005) discuss in detail the different theoretical scenarios that can explain the observations reported in this paper for the BAL-I system of Mrk 231. They found a good agreement between these 2D WHT + INTEGRAL observations of the BAL-I system (plus new X-ray data of BAL QSOs) and the bipolar-jet wind model.

4.3.3 Origin of the variability of the BAL-III system

Boroson et al. (1991) and Kollatschny et al. (1992) have already explained some physical mechanisms that could explain variations in the absorption-line strengths. Here, we reanalyse these and new mechanisms, according to the results obtained in Section 3.

The principal mechanisms that can explain the variability of the Na I D BAL-III system can be listed as follows.

(i) Changes in the intensity of the continuum source (and the ionizing parameter in the absorbing region). Because the continuum flux remained constant in the period in which the system III varied, the first possible explanation can be excluded.

(ii) Changes in the ionizing parameters and density in the absorbing clouds when they move away from the centre. This second possibility has been excluded by Boroson et al. (1991), because the relative change in distance cannot explain the strong change and the systematic increasing and decreasing epochs.

(iii) Motion of absorption clouds with traverse velocity occulting the continuum source. In the past, this was the best explanation for part of the light curve of BAL-III, observed between 1980 and 1992. However, the new observation (presented in Section 3.5) excludes this explanation, because the light-curve fall is clearly asymmetric/exponential.

(iv) An explosive scenario for the origin of the BAL-III system could explain the shape of the light-curve variability, and also the presence of multiple concentric expanding superbubbles/shells (with circular shape). In the next section, we discuss in detail this explosive scenario and the probable origin.

4.3.4 Exploding scenario for Mrk 231 and BAL systems

In Section 3, strong evidence for a composite origin of the OF in the nuclear region of Mrk 231 was detected. Furthermore, for IR mergers/QSOs with EVOF, a similar result was found (for details, see Section 1 and Lípari et al. 2004a,d). Thus, it is important to study whether very energetic explosive events could be originated in the interaction between extreme starbursts and AGNs. We have already explained that Artymowicz et al. (1993) and Collin & Zahn (1999) suggested that the conditions of star formation close to the AGNs + accretion discs could be similar to those of the early/first star formation events, where it is expected that giant explosive processes were generated by giant SNe or HyNe.

Furthermore, it is important to recall that in their study of PG 1700+518, Hazard et al. (1984) have already suggested that high-redshift low-ionization BAL QSOs could be explained by a violent ejection during the first onset of the QSO activity, similar to a 'giant SN explosion'. This approach is very similar to that proposed in this paper for Mrk 231, where 'giant expanding superbubbles' (violent ejection) were found, probably associated – in part – with 'giant' SN or HyN explosions. Therefore, it is important to study in detail the role of giant explosions with OF + superbubble in the origin of some BAL systems and the BLR of Mrk 231 (see Lípari 1994; Lípari et al. 1993, 1994; Dyson, Perry & Williams 1992; Terlevich et al. 1992; Voit, Weymann & Korista 1993).

Recently, one of the most important developments in the study of SNe has been the discovery of some very energetic SNe, whose kinetic energy exceeds 10^{52} erg (HyNe; Paczynski 1998; Galama et al. 1998; Wang 1999; Hjorth et al. 2003). In particular, these HyNe were detected mainly associated with starbursts and long duration gamma-ray bursts (GRBs), e.g. HyN Type Ic 1998bw/GRB 980425, HyN Ic 2003dh/GRB 030329, HyN IIn 1997cy/GRB 970514, HyN IIn 1999E/GRB 980910, HyN IIn 1999eb/GRB 991002, HyN Ic 2003lw/GRB 031203, HyN Ic 2002ap, HyN 1998ey, HyN-NGC 5471B (Galama et al. 1998; Terlevich, Fabian & Turatto 1999; Thorsett & Hogg 1999; Wang 1999; Germany et al. 2000; Hjorth

et al. 2003; Rigon et al. 2003; Malesani et al. 2004; Podsiadlowski et al. 2004). The progenitors of these HyNe are believed to be massive single stars that lost part of their hydrogen and helium envelopes in a strong stellar wind, arising from the collapse of the bare C + O core. These HyNe could be a possible origin for the expanding supergiant bubbles/shells detected in Mrk 231.

For the evolution and explosion of very massive Population III (or primordial) stars, the results of theoretical models suggest that these stars explode as giant HyNe with energies of 10^{53} erg (Heger & Woosley 2002; Heger et al. 2002; Nomoto et al. 2004). This giant HyN with energies up to 100 times that of an ordinary core collapse SN could also be an explanation for the origin of superbubbles. Heiles (1979) has already suggested that this single giant SN or HyN scenario needs to be considered (together with the multiple SN explosion model) in order to study the origin of supergiant bubbles. Thus, this single/few giant HyN scenario is a probable and interesting option to consider for the origin of the expanding supershells, detected in Mrk 231. In particular, in the accretion regions of the AGN, of this merger, the massive stars could be similar to those of very massive Population III stars (Collin & Zahn 1999). Such stars could evolve rapidly toward the giant HyN stage and also could generate multiple expanding superbubbles.

In addition, Park & Vishniac (1991) studied the extreme burst of gravitational radiation which results from the merger of massive black holes; they also called these bursts giant HyNe. They proposed that the extreme case of these giant bursts could be detected in the very nucleus of galaxy mergers, because in these systems we expect the merger between the cores + SMBH from the original galaxies that collide (plus their satellites/companions). Recently, using a hydrodynamical simulation for the study of the growth of SMBHs in mergers, Springel, Di Mateo & Hernquist (2005) found that the SMBH can drive powerful winds/explosions once the black hole becomes sufficiently massive (see also King 2003; King & Pounds 2003). Thus, there are other possible origins for some of the expanding superbubbles found in Mrk 231.

Very recently, Miller, Reynolds & Krishnamurthi (2005) proposed that extreme OFs are the main event capable of stopping the growth of SMBHs. In particular, these OF events could stop – and expel – the gas falling toward the black hole, and thus can control the final mass of SMBHs. Furthermore, they also suggested that these giant OF processes could stop the cooling flow in the central members/regions (M87 and NGC 1275) of the Virgo and Perseus clusters of galaxies. Thus, giant OFs associated with explosive events and jets could play a main role in the growth of SMBHs.

For the origin of BAL systems in QSOs/AGNs, in the composite starburst + AGN + GW scenario, different theoretical models were proposed, in particular the following. (i) In SN or HyN ejecta (close to AGN + GW), which are shock-heated when a fast forward shock moves out into the ISM (with a velocity roughly equal to the ejecta) and a reverse shock accelerates back and moves towards the explosion centre, the blue absorption lines arise because SN debris moving toward the central source are slowed down much more rapidly – by the AGN wind – than material is moving away (Perry & Dyson 1992; Perry 1992). (ii) For IR dusty QSOs + GW, in the outflowing gas + dust material the presence of discrete trails of debris (shed by individual mass-loss stars) could produce the BAL features (Scoville & Norman 1995).

The presence of large galactic-scale OF, superbubbles in IR QSOs could be a third explanation – in a composite scenario – for the origin of BAL systems in these objects (see Lípari 1994; Guillemin & Bergeron 1997; Bond et al. 2001). In particular, interesting results were obtained by Tenorio-Tagle et al. (1999), who studied a scenario based on the hydrodynamics of superbubbles/GWs powered by massive starbursts that account for different types of BAL systems detected in star-forming galaxies (Kunth et al. 1998; Mas-Hesse et al. 2003). These types of starburst models could explain part of the BAL systems detected in Mrk 231; however, in this merger, probably the nuclear extreme starburst and the GW are strongly associated with the QSO/AGN (in agreement with the evolution of massive star formation process in the accretion regions of AGNs/QSOs; proposed by Collin & Zahn 1999). In this last scenario the presence of HyN explosions is expected.

On the other hand, different works proposed that even the BLR could be associated with OF processes. In particular, these works suggest that the BLRs are located in the OF of accretion discs, the ejecta of SN remnants, shocked clouds (by a nuclear GW) around SN remnants, extended stellar envelopes, etc. (for references/review, see Scoville & Norman 1988; Dyson, Perry & Williams 1992; Terlevich et al. 1992; Sulentic, Marziani & Dultzin-Hacyan 2000, respectively). Thus, an interesting questions is, could an explosive event generate a very unusual spectrum similar to that detected in the nuclear region of Mrk 231?. Fig. 14 shows the superposition of the spectrum of the unusual radio SN type IIL 1979c (observed on 1979 June 26.18; Branch et al. 1981). Only using colours, we can distinguish each spectrum, because they are almost identical. Thus, a more constant OF (than a single/standard SN) could explain even the optical spectrum of the BLR in Mrk 231.

Finally, we remark that it is important that a high number of QSOs have been detected that show BAL systems at low redshift (in IR + Fe II emitters) and at very high redshift (in Fe II emitters; Maiolino et al. 2003, 2004a). However, the relation between BAL, IR, GW and Fe II emission is not well understood. Fe II emission (with low-ionization level) could originate in warm regions, and is thus obscured from the direct ionizing UV photons. In the case of strong Fe II emitters, the obscuring material may be in the form of an expanding supershell. If so, BAL + Fe II + IR objects are not ordinary AGNs; rather, they may be associated with early starburst activities. If some absorptions are the result of outbursts, the mass involved should be much larger than a typical SN, because the Fe II emission and 'some' BAL systems do not fall in years. However, in order to understand this type of giant outburst (i.e. from HyN or giant SN explosions from very massive stars, Population III stars, etc.), more detailed theoretical studies are required. The results found in this paper for Mrk 231 (and similar IR QSOs) support the reality of these giant explosive processes.

4.4 Mrk 231 and extreme IR + GW/OF + Fe II + BAL QSOs as transition/young quasi-stellar objects

In this section, we analyse the properties of Mrk 231 together with the other members of the interesting group of IR + GW/OF + Fe II + BAL transition/young QSOs.

4.4.1 Infrared colour diagram for a small sample of IR + GW/OF + Fe II + BAL quasi-stellar objects

In general, the *IRAS* colour–colour diagrams have been used as an important tool to detect and discriminate different types of activity in the nuclear/circumnuclear regions of galaxies (e.g. Seyfert and starburst activity; see de Gripj et al. 1985; de Gripj, Miley & Lub 1987; Sekiguchi 1987; Rowan-Robinson & Crawford 1989). Lípari (1994) already found that the IR colours (i.e. IR energy distribution) of ∼10 extreme IR + Fe II QSOs (e.g. Mrk 231, IRAS 07598+6508, IRAS 17002+5153, IRAS 14026+4341, IRAS 00275−2859, I Zw 1, IRAS 18508−7815, IRAS 21219−1757, Mrk 507, Mrk 957, etc.)

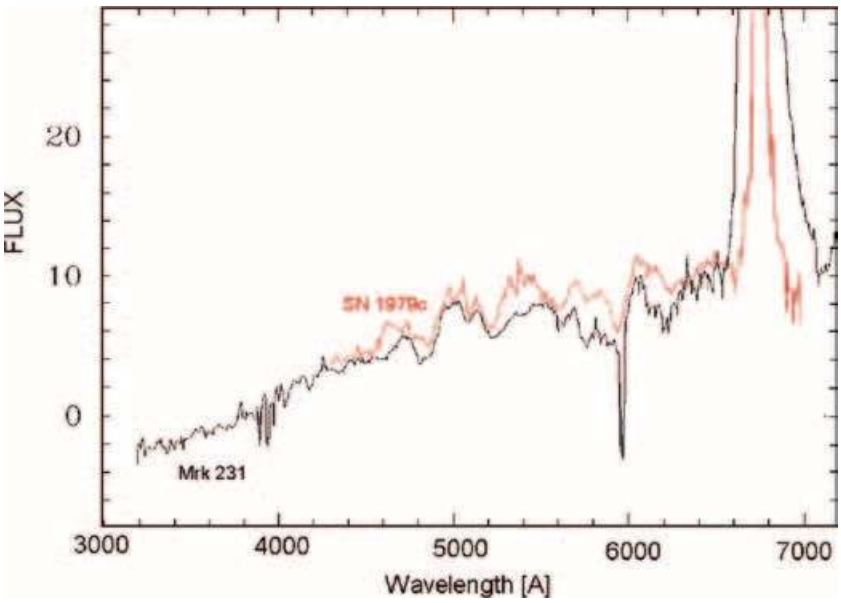

Figure 14. Optical spectrum of Mrk 231 superposed to the spectrum of the SN 1979c (Branch et al. 1981).

are distributed between the power-law and the blackbody regions (i.e. the transition area). On the other hand, the low and moderate IR–Fe II emitters are located mainly in the power-law region.

In particular, we detected that Mrk 231 and IRAS 07598+6508 (the nearest IR + GW/OF + Fe II + BAL QSOs) have a close position in this diagram, near to the blackbody area, thus showing both systems to be strong starburst components. Recently, Canalizo & Stockton (2001) confirmed that the host galaxies of both QSOs have strong starburst populations (using Keck spectroscopy). In general, the QSOs with extreme Fe II + IR emission show weaker 'Seyfert/AGN' components than the low/moderate Fe II emitters.

Furthermore, we found that the IR properties/colours of narrow-line Seyfert 1 IR AGNs with extreme Fe II emission (such as Mrk 507 and Mrk 957) also lie in the transition area between the blackbody and power-law regions, and close to standard disc galaxies (Rowan-Robinson & Crawford 1989) and starburst objects (Sekiguchi 1987).

It is important to note that of a total of ∼10 IR transition objects of this original sample, the first four systems are BAL IR QSOs. Therefore, we have already suggested that BALs IR QSOs (such as Mrk 231, IRAS 07598+6508, IRAS 17002+5153 and IRAS 14026+4341) could be associated with the young phase of the QSO activity.

4.4.2 Infrared colour diagram for a large sample of infrared mergers and infrared quasi-stellar objects with galactic winds

In this paper, using our data base of more than 50 IR mergers and QSOs with GWs and using for comparison the large sample of standard PG QSO (from Boroson & Green 1992) we expand our previous study. Fig. 15 and Table 1 show the IR energy distribution – spectral indexes $\alpha(60, 25)$ versus $\alpha(100, 60)$, where $\alpha(\lambda 2, \lambda 1) = -\log[F(\lambda 2)/F(\lambda 1)]/\log[\lambda 2/\lambda 1]$ – for (i) IR mergers and IR QSOs with GWs (originally 51 IR systems, from Table 1), and (ii) standard QSOs from the PG QSO sample of Boroson & Green (1992), originally 87 PG QSOs that have $z \leqslant 0.5$.

IR fluxes–densities, in the bands of 12, 25, 60 and 100 μm, were obtained from the *IRAS* and *ISO* Archival Catalogue, using the NASA/IPAC Extragalactic Database (NED). Only objects with a good detection in the three required bands have been included. Also, the localization of the three main regions in this colour–colour diagram (i.e. the QSOs/Seyferts, starbursts and powerful IR galaxy areas) have been plotted. An inspection of this diagram clearly shows the following.

(i) All the IR mergers with LVOF are located very close to the blackbody and starburst area.

(ii) Almost all the IR QSOs with EVOF are located in the transition region.

The only object, NGC 3079, not following this trend is the only spiral galaxy in this sample.

(iii) The standard QSOs and radio QSOs are located around the power-law region.

(iv) All the BAL IR QSOs are located in the transition region, in almost a clear sequence: from Mrk 231 (close to the blackbody area) → IRAS 07598+6508 → IRAS 21219−1757 → IRAS/PG 17072+5153 and IRAS 14026+4341 (close to the power-law area) → standard QSOs.

Therefore, these results confirm our previous finding (obtained from a small sample of IR galaxies): in the sense that IR QSOs are probably 'transition' objects, between IR mergers and standard QSOs. However, it is important to remark that more detailed studies of individual IR systems (such as Mrk 231) are required in order to determine the different paths of possible evolution (see Farrah et al. 2001; Rigopoulou et al. 1999).

4.4.3 IRAS 04505−2958: an IR + GW/OF + Fe II + BAL quasi-stellar object rosetta?

It is important to remark that in Fig. 15 IRAS 04505−2958 is located exactly in the sequence of BAL QSOs, between the positions of IRAS 07598+6508 and IRAS 21219−1757. This IR + GW + Fe II QSO shows probably the more interesting OF supershell/arc detected to date. This is very extended (of ∼20–25 kpc) and it is located very far from the nucleus (at $r \sim 15$ kpc; for details, see Fig. 16a). Thus, this very extended supershell could be associated with a hyperwind (see Taniguchi & Shioya 2000 for references to hyperwinds).

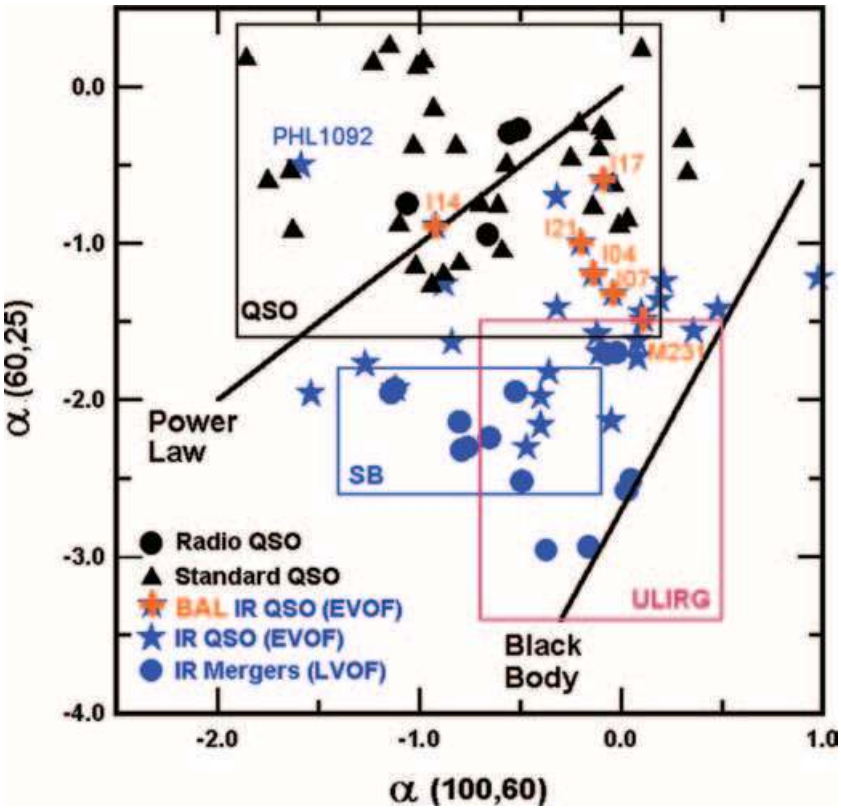

Figure 15. IR colour–colour diagram for IR mergers/QSOs with GWs (from Table 1 of this paper) and for standard QSOs (from the PG sample; Boroson & Green 1992).

The UV *HST* FOS spectra of IRAS 04505−2958 clearly show a BAL system at the C IVλ1549 emission line (Figs 16b and c). For this BAL system we measured $\lambda = 1978.5$ Å, corresponding to an ejection velocity of -1645 km s^{-1}. This ejection velocity is (within the errors) the same as the previous value of OF obtained using the offset method, -1700 km s^{-1} (by Lípari et al. 2004d).

The offset method used for the study of OF candidate IR QSOs (including IRAS 04505−2958) means that the Hβ broad line component is blueshifted in relation to the narrow one. Thus, this result obtained for IRAS 04505−2958 suggests that the optical low-ionization BLR and the BAL could originate in the same OF process or supershells.

Finally, the more complete sequence of BAL + IR + Fe II QSOs (derived from Fig. 15) is: from Mrk 231 (close to the blackbody area) → IRAS 07598+6508 → IRAS 04505−2958 → IRAS 21219−1757 → IRAS/PG 17072+5153 and IRAS 14026+4341 (close to the power-law area) → standard QSOs.

4.4.4 Possible relation between IR + GW/OF + Fe II + BAL transition/young quasi-stellar objects and very high-redshift broad absorption line quasi-stellar objects

It has been proposed that extreme starburst + GW processes associated with IR mergers could play a relevant role in the formation and evolution of galaxies and QSOs/AGNs (i.e. in their structure, kinematics, metallicity, etc.; see Section 1 for references). Furthermore, recent detailed observations and theoretical studies have confirmed that OF, GW, BAL, the large amount of gas + dust and strong Fe II emission are important components and processes at high redshift ($z \sim 4$–6), when galaxies and QSOs formed (Taniguchi & Shioya 2000; Omont et al. 2001; Pettini et al. 2001; Ajiki et al. 2002; Dawson et al. 2002; Frye, Broadhurst & Benitez 2002; Iwamuro et al. 2002; Barth et al. 2003; Bertoldi et al. 2003a,b; Freudling, Corbin & Korista 2003; Solomon, Vaden Bout & Guelin 2003; Carilli et al. 2004a,b; Maiolino et al. 2004a,b).

Specifically, cm and mm observations of thermal molecular line emission from high-redshift QSOs reveal massive gas reservoirs (10^{10}–10^{11} M$_\odot$) required to fuel extreme star formation (Carilli, Menten & Yun 1999; Carilli & Blain 2002; Solomon et al. 2003; Carilli et al. 2004a,b). In addition, cm and mm observations also reveal in high-redshift QSOs a very large amount of dust of 10^8 M$_\odot$. The presence of this large mass of dust is associated mainly with massive starbursts concurrent with AGNs, which implies star formation rates greater than 10^3 M$_\odot$ yr^{-1} (Carilli et al. 2000; Omont et al. 2001; Cox et al. 2002; Bertoldi et al. 2003a,b).

On the other hand, Maiolino et al. (2004a) presented near-IR spectra of eight of the more distant QSOs (at $4.9 < z < 6.4$). Half of these QSOs are characterized by strong UV BAL systems (at C IV, Mg II, Si IV, Al III lines). Although the sample is small, the large fraction of BAL QSOs suggests that the accretion of gas, the amount of dust and the presence of OF process are larger (in these objects) than in standard QSOs at $z < 4.0$. They also suggest that the very high amount of dust was generated by early explosions of SNe (Maiolino et al. 2004b).

Finally, it is important to note the similar properties found in IR + GW/OF + Fe II + BAL QSOs at low redshift (such as Mrk 231) and very high-redshift BAL QSOs (at $z \sim 6.0$; Maiolino et al. 2003, 2004a,b; Carilli et al. 2004a,b). According to these similarities, we propose that the phase of a young QSO could be associated with the following main processes.

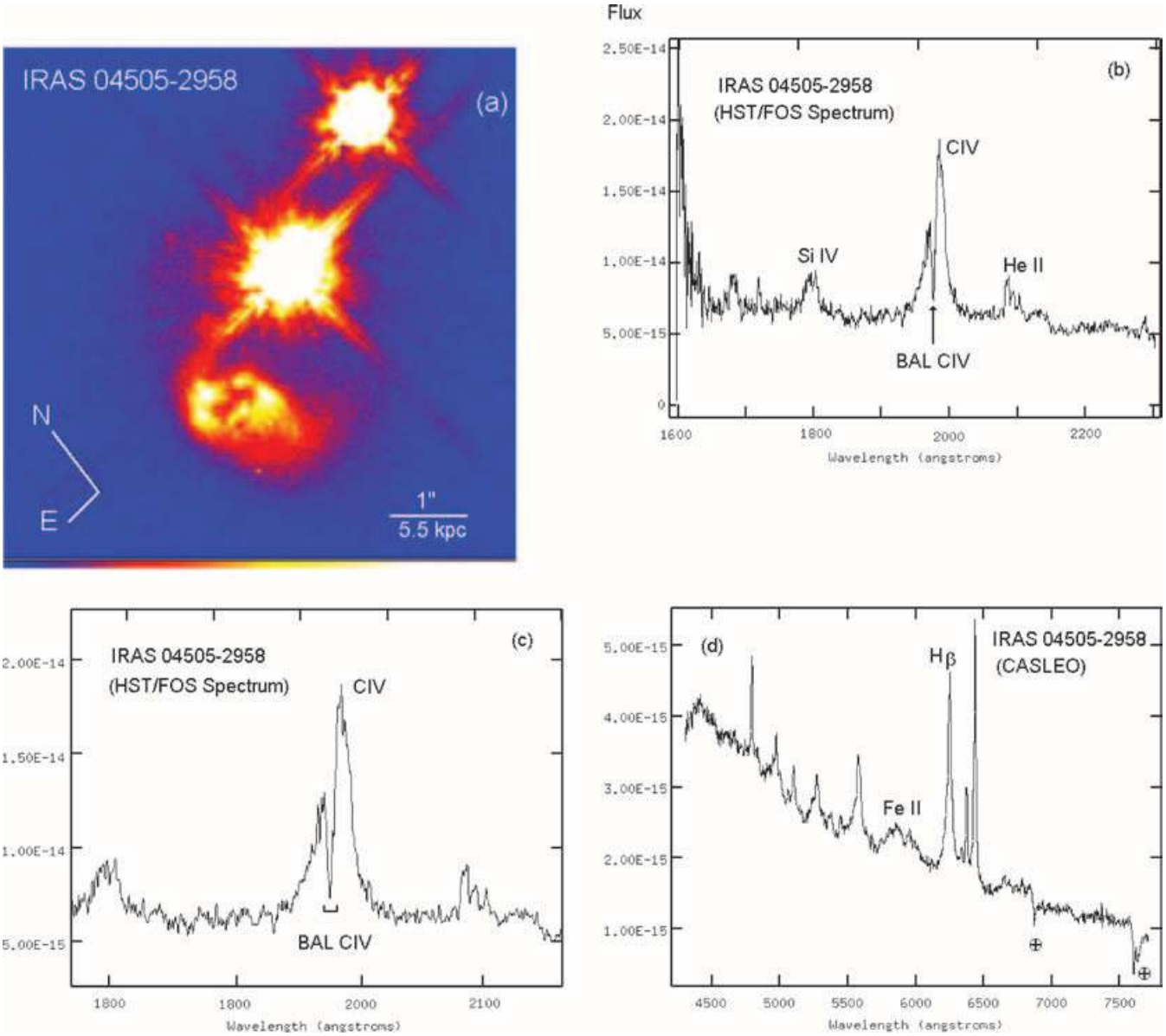

Figure 16. *HST* WFPC2 optical image of IRAS 04505−2958, through the filter F702W (a). *HST* FOS UV spectra, for the region of C IV (b), (c). CASLEO optical spectra (d). The scales of flux (in the spectra) are given in units of erg cm^{-2} s^{-1} Å^{-1}.

(i) In young QSOs with an extremely large amount of gas (concentrated in their nuclear region), the accretion rate of gas – by the SMBH – could be extremely high (see Maiolino et al. 2004a).

(ii) In addition, this extremely large amount of molecular gas could generate extreme starbursts, and the presence of AGNs could increase the star formation close to the nucleus, especially in the accretion discs, with properties – of the star formation – similar to Population III stars. In these extreme starbursts – closely associated with QSOs/AGNs – giant SN or HyN explosions are expected.

(iii) In young and distant QSOs, the very high number of BAL detections suggest that composite OFs (or EVOFs) play a main role in their evolution.

Furthermore, this scenario is in close agreement with the results of the study of proto-QSO evolution and black hole growth (using hydrodynamic models). In particular, Kawakatu, Umemura & Mori (2003) found that a ULIRG phase (where the host galaxy is the dominant source of luminosity, i.e. IR galaxies/mergers with starbursts) precedes a GW epoch (i.e. composite young IR + OF/GW + BAL mergers/QSOs). This would be a transition state to the AGN-dominated phase (i.e. the standard QSO phase). This evolutive path is almost identical to the sequence found for BAL IR + Fe II QSOs, in Fig. 15.

5 SUMMARY AND CONCLUSIONS

We have presented in this paper optical 2D and 1D spectroscopy (obtained at La Palma/WHT, *HST*, *IUE*, ESO/NTT, KPNO, APO and CASLEO observatories) and deep *HST* broad-band images of Mrk 231 and similar IR + GW/OF + Fe II QSOs. The main results and conclusions can be summarized as follows.

(i) We have presented a detailed study of the kinematics, morphology, physical conditions and ionization structure of the extreme galactic superwind + superbubble (detected previously in the nuclear and central regions of the IR merger/QSO Mrk 231). This study

is based mainly on 2D INTEGRAL spectroscopy (obtained at the La Palma 4.2-m WHT) plus *HST* near-UV/ACS, optical/WFPC2 and near-IR/NICMOS broad-band images.

(ii) Inside and very close to the nucleus, the 2D spectra show the presence of an OF emission bump in the blend Hα+[N II], with a peak at the same velocity as the main BAL-I system ($V_{\rm Ejection\,BAL-I} \sim -4700$ km s^{-1}). This bump was more clearly detected in the area located at 0.6–1.5 arcsec (490–1220 pc), to the south-west of the nucleus core, showing a strong and broad peak. In addition, in the same direction (at PA $\sim -120^{\circ}$, i.e. close to the PA of the small- scale radio jet) at 1.7–2.5 arcsec (1340–2030 pc), we also detected multiple narrow emission-line components, with a 'greatly' enhanced [N II]/Hα ratio (very similar to the spectra of bow shocks in jets, already found in the Circinus galaxy). Thus, these results suggest that probably the BAL-I system is generated in OF clouds associated with the parsec-scale jet.

(iii) The *HST* images show four (or five) nuclear superbubbles or shells with radii $r \sim 2.9$, 1.5, 1.0, 0.6 and 0.2 kpc (3.5, 1.8, 1.2, 0.7 and 0.3 arcsec). For these bubbles, the 2D Hα VF map and 2D spectra show the following. (i) At the border of the more extended superbubble or shell (S1), a clear expansion of the shell with blueshifted velocities (with circular shape and at a radius $r \sim 3.0$ arcsec). This superbubble shows a rupture arc – to the south – suggesting that the bubble is in the blowout phase. The axis of this rupture or ejection (at PA $\sim 00^{\circ}$) is coincident with the axis of the intermediate and large-scale OF detected at radio wavelengths ($r \sim 0.6$ arcsec ~ 50.0 pc at 2.3 GHz, and $r \sim 30.0$ arcsec ~ 25.0 kpc at 1.5 GHz). (ii) In addition, in the three more external superbubbles (S1, S2, S3), the 2D WHT spectra show multiple emission-line components with OF velocities, of $\langle V_{\rm OF\,Bubble-S1}\rangle = [-(650 - 420) \pm 30]$ km s^{-1}, $\langle V_{\rm OF\,Bubble-S2}\rangle = [-500 \pm 30]$ km s^{-1} and $\langle V_{\rm OF\,Bubble-S3}\rangle = [-230 \pm 30]$ km s^{-1}. (iii) In the whole circumnuclear region ($1.8 < r < 5$ arcsec), the [N II]/Hα and [S II]/Hα narrow emission-line ratios show high values (>0.8), which are consistent with OF processes associated with fast velocity shocks. Therefore, we suggest that these supergiant bubbles are associated with the large-scale nuclear OF component, which is generated – at least in part – by the extreme nuclear starburst (i.e. Type II SN explosions).

(iv) High-resolution *HST* ACS, WFPC2 and NICMOS broad-band images (using the filters F330W, F439W $\sim B$, F814W $\sim I$ and F160W $\sim H$) were combined with the 2D WHT spectra to study the physical properties of the multiple superbubbles/shells. In particular, we study the properties of several blue/young star-forming regions, located mainly at the border of these shells.

(v) Finally, the variability of the short-lived BAL-III Na I D system was studied, covering almost the whole period in which this system appeared (between ~1984 and 2004). We found that the BAL-III light curve is clearly asymmetric with a steep increase, a clear maximum and an exponential fall (similar to the shape of an SN light curve). Previously, the nature of this light curve was discussed assuming a symmetric or Gaussian form. In this paper we discuss the origin of this BAL-III system, mainly in the framework of an extreme explosive event (at parsec scale), probably associated with giant SNe or HyNe, with very massive star progenitors and located close to the AGN and/or in an accretion disc.

Using our data base for more than 50 IR mergers and QSOs with GWs and using for comparison the large sample of standard PG QSOs (from Boroson & Green 1992), we confirm our previous finding (obtained from a small sample of IR galaxies), in the sense that IR QSOs are probably 'transition' objects, between IR mergers and standard QSOs.

Finally, we analysed new observations of UV–BAL systems of IR + GW/OF + Fe II QSOs. This study shows two new BAL IR QSOs and suggests/confirms that these objects could be nearby young BAL QSOs, similar to those detected recently at $z \sim 6.0$. We propose that the phase of the young QSO is associated with accretion of a large amount of gas (by the SMBH) + extreme starbursts + extreme composite OFs/BALs.

ACKNOWLEDGMENTS

The authors thank J. Acosta, J. Ahumada, R. Antonucci, C. Beauge, K. Chiu, H. Dottori, R. Diaz, J. C. Forte, H. Levato, E. Mediavilla, D. Merlo, B. Punsly and Z. Tsvetanov for assistance and constructive discussions. We wish to thank T. Boroson, R. Green, D. Kim, D. Macchetto, D. Sanders, Z. Tsvetanov, S. Veilleux and M. Veron for their 1D spectra, kindly made available to us. This paper is based on observations obtained at La Palma/WHT, *HST*, *IUE*, ESO/NTT, KPNO, APO and CASLEO. The 4.2-m WHT is operated by the Issac Newton Group at the Observatorio de Roque de los Muchachos of the Instituto de Astrofisica de Canarias. The APO observations were obtained with the 3.5-m telescope, which is owned and operated by the Astrophysical Research Consortium. The authors thank all the staff at La Palma, ESO, KPNO, APO and CASLEO observatories, for their kind support. This work was based on observations made using the National Aeronautics and Space Administration (NASA) and European Space Agency *HST*, obtained from archive data at the ESO Garching and the Space Telescope Science Institute Baltimore. This work was carried out using the NED, which is operated by the Jet Propulsion Laboratory, California Institute of Technology, under contract with NASA. This work was supported in part by grants from Conicet, SeCyT-UNC and Fundación Antorchas (Argentina).

REFERENCES

Adams T. F., 1972, ApJ, 176, L1
Adams T. F., Weedman D. W., 1972, ApJ, 172, L19
Aguirre A., Hernquist L., Schaye J., Katz N., Weinberg D., Gardner J., 2001, ApJ, 561, 521
Ajiki M. et al., 2002, ApJ, 576, L25
Arakelian M. A., Debai E., Esipov V., Markarian B., 1971, Astrophyzika, 7, 177
Armus L., Surace J. A., Soifer B. T., Matthews K., Graham J. R., Larkin J. E., 1994, AJ, 108, 76
Arribas S. et al., 1998, Proc. SPIE, 3355, 821
Artymowicz P., Lin D., Wampler E., 1993, ApJ, 409, 592
Barth A., Martini P., Nelson C., Ho L., 2003, ApJ, 594, L95
Baum S., O'Dea C., Dallacassa D., de Bruyn A., Pedlar A., 1993, ApJ, 419, 553
Bertoldi F. et al., 2003a, A&A, 409, L47
Bertoldi F., Carilli C. L., Cox P., Fan X., Strauss M. A., Beelen A., Omont A., Zylka R., 2003b, A&A, 406, L55
Bevington P., 1969, Data Reduction and Error Analysis for the Physical Sciences. McGraw-Hill, New York
Bicknell G., Dopita M. A., Tsvetanov Z. I., Sutherland R. S., 1998, ApJ, 495, 680
Bingham R., Gellatly D. W., Jenkins C. R., Worswick S. P., 1994, Proc. SPIE, 2198, 56
Boksenberg A., Carswell R., Allen D., Fosbury R., Penston M., Sargent W., 1977, MNRAS, 178, 451
Bond N., Churchill C., Charlton J., Vogt S., 2001, ApJ, 562, 641
Boroson T., Green R., 1992, ApJS, 80, 109
Boroson T., Meyers K., 1992, ApJ, 397, 442
Boroson T., Meyers K., Morris S., Persson S., 1991, ApJ, 370, L19
Branch D., Falk S., McCall M., Rybski P., Uomoto A., 1981, ApJ, 244, 780

Bryant P., Scoville N., 1996, ApJ, 457, 678
Bromm V., Loeb A., 2003, Nat, 425, 812
Bromm V., Coppi P., Larson R., 1999, ApJ, 527, L5
Canalizo G., Stockton A., 1997, ApJ, 480, L5
Canalizo G., Stockton A., 2001, ApJ, 555, 719
Canalizo G., Stockton A., Roth K., 1998, AJ, 115, 890
Cappeti A., 2002, in Henney W. Saffe W., Raga A., Binette L. eds., Emission Lines from Jets Flows, UNAM Mexico. RevMexAA Ser. Conf. 13, 163
Carilli C., Blain A., 2002, ApJ, 569, 605
Carilli C., Wrobel J., Ulvestad J., 1998, AJ, 115, 928
Carilli C., Menten K., Yun M., 1999, ApJ, 521, L25
Carilli C. et al., 2000, ApJ, 533, L13
Carilli C. et al., 2004a, AJ, 128, 997
Carilli C., Bertoldi F., Walter F., Menten K., Beelen A., Cox P., Omont A., 2004b, in Mújica A., Maiolino R., eds, Multiwavelength AGN Surveys. World Scientific, Singapore
Cecil G., Ferruit P., Veilleux S., 2002, in Henney W., Saffe W., Raga A., Binette L., eds, Emission Lines from Jets Flows, UNAM Mexico. RevMexAA Ser. Conf., 13, 170
Chevalier R., Clegg A., 1985, Nat, 317, 44
Clements D., Sutherland W. J., Saunders W., Efstathiou G. P., McMahon R. G., Maddox S., Lawrence A., Rowan-Robinson M., 1996, MNRAS, 279, 459
Colina L., Lípari S. L., Macchetto F., 1991, ApJ, 379, 113
Colina L., Arribas S., Borne K., 1999, ApJ, 527, L13
Colina L. et al., 2001, ApJ, 563, 546
Collin S., Zahn P., 1999, A&A, 344, 433
Condon J., Huang Z., Yin Q., Thuan T., 1991, ApJ, 378, 65
Cox P. et al., 2002, A&A, 387, 406
Cutri R., Rieke G., Lebofsky M., 1984, ApJ, 287, 566
Davies R., Tacconi L., Genzel R., 2004, ApJ, 613, 781
Dawson S., Spirand H., Stern D., Day A., van Breugel W., Vries W., Reuland M., 2002, ApJ, 570, 92
de Kool M., Arav N., Becker R., Gregg M., White R., Laurent-Muehleisen S., Price T., Korista K., 2001, ApJ, 548, 609
de Kool M., Becker R., Arav N., Gregg M., White R., 2002, ApJ, 570, 514
de Gripj M., Miley G., Lub J., Joung T., 1985, Nat, 314, 240
de Gripj M., Miley G., Lub J., 1987, A&AS, 70, 95
Dekel A., Silk J., 1986, ApJ, 303, 39
Dietrich M., Appenzeller I., Vestergaard M., Wagner S., 2002, ApJ, 564, 581
Dopita M., 1994, in Bicknell G., Dopita M., Quin P., eds., ASP Conf. Ser. Vol. 54, The Physics of Active Galaxies. Astron. Soc. Pac., San Francisco, p. 287
Dopita M., Sutherland R., 1995, ApJ, 455, 468
Downes D., Solomon P. M., 1998, ApJ, 507, 615
Dyson J., Perry J., Williams R., 1992, in Holt S., Neff S., Urry M., eds, Testing the AGN Paradigm. AIP, New York, p. 548
Egami E., Iwamuro F., Maihara T., Oya S., Cowie L., 1996, AJ, 112, 73
Farrah D. et al., 2001, MNRAS, 326, 1333
Ferrarese L., Merrit D., 2000, ApJ, 539, L9
Forster K., Rich M., McKarthy J., 1995, ApJ, 450, 74
Freudling W., Corbin M., Korista K., 2003, ApJ, 587, L67
Frye B., Broadhurst T., Benitez N., 2002, ApJ, 568, 558
Galama T. et al., 1998, Nat, 395, 670
Gallagher E., Brandt W., Chartas G., Garmire G., Sambruna R., 2002, ApJ, 569, 655
Gebhardt K. et al., 2000, ApJ, 539, L13
Genzel R. et al., 1998, ApJ, 498, 579
Genzel R., Tacconi L., Rigopoulou D., Lutz D., Tecza M., 2001, ApJ, 563, 527
Germany L., Reiss D., Schmidt B., Stubbs C., Sadler E., 2000, ApJ, 533, 320
Guillemin P., Bergeron J., 1997, A&A, 328, 499
Hamilton D., Keel W., 1987, ApJ, 321, 211
Hazard C., Morton D., Terlevich R., McMahon R., 1984, ApJ, 282, 33
Heckman T. M., 1980, A&A, 87, 152
Heckman T. M., 1996, in Eracleous M., Koratkar A., Leitherer C., Ho L., eds, ASP Conf. Ser. Vol. 103, The Physics of LINERs in View of Recent Observations. Astron. Soc. Pac., San Francisco, p. 241
Heckman T. M., Armus L., Miley G., 1987, AJ, 93, 276
Heckman T. M., Armus L., Miley G., 1990, ApJS, 74, 833
Heckman T. M., Lehnert M., Strickland D., Armus L., 2000, ApJS, 129, 493
Heger A., Woosley S., 2002, ApJ, 567, 532
Heger A., Woosley S., Baraffe I., Abel T., 2002, in Gilfanov M., Sunyaev R., Curazov E., eds, Ligthhouses of the Universe: The Most Luminous Celestial Objects and Their Use in Cosmology. Springer-Verlag, Berlin, p. 369 (astro-ph/0112059)
Heger A., Fryer C., Woosley S., Langer N., Hartmann D., 2003, ApJ, 591, 288
Heiles C., 1979, ApJ, 229, 533
Hines D., Wills B., 1995, ApJ, 448, L69
Hjorth J. et al., 2003, Nat, 423, 847
Hutching J., Neff S., 1987, AJ, 93, 14
Ikeuchi S., Ostriker J., 1986, ApJ, 301, 522
Iwamuro F., Mtohara K., Maihara T., Kimura M., Yoshi Y., Doi M., 2002, ApJ, 565, 63
Joseph R. D., Wright G., 1985, MNRAS, 214, 87
Kauffmann G., Charlot S., 1998, MNRAS, 294, 705
Kawakatu M., Umemura M., Mori M., 2003, ApJ, 583, 85
King A., 2003, ApJ, 596, L27
King A., Pounds K., 2003, MNRAS, 345, 657
Kollatschny W., Dietrich M., Hagen H., 1992, A&A, 264, L5
Kormendy J., 2000, Sci, 289, 1484
Kormendy J., Richstone D., 1995, ARA&A, 33, 581
Krabbe A., Colina L., Thatte N., Kroker H., 1997, ApJ, 476, 98
Kunth D., Mas-Hesse J., Terlevich E., Terlevich R., Lequeux J., Fall M., 1998, A&A, 334, 11
Lanzetta K., Turnshek D., Sandoval J., 1993, ApJS, 84, 109
Larson R., 1974, MNRAS, 166, 585
Larson R., 1998, MNRAS, 301, 569
Larson R., 1999, in Favata F., Kaas A., Wilson A., eds, ESA SP-445, Star Formation from the small to the large scale. ESA, Noordwijk, p. 13
Larson R., 2003, Rep. Prog. Phys., 66, 1651 (astro-ph/0306595)
Lawrence A., Elvis M., Wilkes B. J., McHardy I., Brandt N., 1997, MNRAS, 285, 879
Lípari S. L., 1994, ApJ, 436, 102
Lípari S. L., Macchetto F., Golombeck D., 1991a, ApJ, 366, L65
Lípari S. L., Bonatto Ch., Pastoriza M., 1991b, MNRAS, 253, 19
Lípari S. L., Terlevich R., Macchetto F., 1993, ApJ, 406, 451
Lípari S. L., Colina L., Macchetto F., 1994, ApJ, 427, 174
Lípari S. L., Tsvetanov Z., Macchetto F., 1997, ApJS, 111, 369
Lípari S. L., Diaz R., Taniguchi Y., Terlevich R., Dottori H., Carranza G., 2000a, AJ, 120, 645
Lípari S. L. et al., 2000b, preprint (astro-ph/0007316)
Lípari S. L., Terlevich R., Diaz R., Taniguchi Y., Zheng W., Tsvetanov Z., Carranza G., Dottori H., 2003, MNRAS, 340, 289
Lípari S. L., Mediavilla E., Diaz R., Garcia-Lorenzo B., Acosta-Pulido J., Agüero M., Terlevich R., 2004a, MNRAS, 348, 369
Lípari S. L. et al., 2004b, in Storchi Bergmann T., Ho L., Schmitt H., eds, IAU Symp. No. 222, ASP Conf. Ser., The Interplay among Black Hole Stars and IGM in Galactic Nuclei. Astron. Soc. Pac., San Francisco, p. 529
Lípari S. L. et al., 2004c, MNRAS, 354, L1
Lípari S. L. et al., 2004d, MNRAS, 355, 641
Lonsdale C. J., Lonsdale C. J., Smith H., Diamond P., 2003, ApJ, 592, 804
Low F., Cutri R., Kleinmann S., Huchra J., 1989, ApJ, 340, L1
Mac Low M., McCray R., Norman M., 1989, ApJ, 337, 141
Magorrian J. et al., 1998, AJ, 115, 2285
Maiolino R., Juarez Y., Mujica R., Nagar N., Oliva E., 2003, ApJ, 596, L155
Maiolino R., Oliva E., Ghinassi F., Pedani M., Mannucci F., Mujica R., Juarez Y., 2004a, A&A, 420, 889
Maiolino R., Schneider R., Oliva E., Bianchi S., Ferrara A., Mannucci F., Pedani M., Roca Sogorb M., 2004b, Nat, 431, 533
Malesani D. et al., 2004, ApJ, 609, L5
Markarian B. E., 1969, Astrophyzika, 5, 286

Mas-Hesse J., Kunth D., Tenorio-Tagle G., Leitherer C., Terlevich R., Terlevich E., 2003, ApJ, 598, 858
Mathews W., Baker J., 1971, ApJ, 170, 241
Melnick J., Mirabel I. F., 1990, A&A, 231, L19
Mendes de Oliveira C., Plana H., Amram P., Bolte M., Boulesteix J., 1998, ApJ, 507, 691
Merrit D., Ferrarese L., 2001, MNRAS, 320, L30
Miller M., Reynolds C., Krishnamurthi A., 2005, S&T, 109(4), 42
Morganti R., Oosterloo T., Emonts B., van der Hulst J., Tadhunter C., 2003, ApJ, 593, L69
Murray N., Chiang J., Grossman S. A., Voit G. M., 1995, ApJ, 451, 498
Neff S., Ulvestad J., 1988, AJ, 96, 841
Nomoto K., Maeda K., Mazzali A., Umeda H., Deng J., Iwamoto K., 2004, in Fryer C., ed., Stellar Colapse. Kluwer, Dordrecht, p. 277
Norman C., Ikeuchi S., 1989, ApJ, 395, 372
Norman C., Miley G., 1984, A&A, 141, 85
Omont A., Cox P., Bertoldi F., McMahon R. G., Carilli C., Isaak K. G., 2001, A&A, 374, 371
Ostriker J., Cowie L., 1981, ApJ, 243, L127
Paczynski B., 1998, ApJ, 494, L45
Park S., Vishniac E., 1991, ApJ, 375, 565
Perry J., 1992, in Filippenko A., ed., ASP Conf. Ser. Vol. 31, Relationships Between AGN and Starburst Galaxies. Astron. Soc. Pac., San Francisco, p. 169
Perry J., Dyson R., 1992, in Holt S., Neff S., Urry M., eds, Testing the AGN Paradigm. AIP, New York, p. 553
Pettini M., Shapley A., Steidel C., Cuby J., Dickinson M., Moorwood A., Adelberg K., Giavalisco M., 2001, ApJ, 554, 981
Podsiadlowski Ph., Mazzali P., Nomoto K., Lazzati D., Cappellaro E., 2004, ApJ, 607, L17
Preuss E., Fosbury R., 1983, MNRAS, 204, 783
Proga D., Stone J., Kallman T., 2000, ApJ, 543, 686
Punsly B., 1999a, ApJ, 527, 609
Punsly B., 1999b, ApJ, 527, 624
Punsly B., Lípari S., 2005, ApJ, 623, L101
Quillen A., McDonald C., Alonzo-Heerrero A., Lee A., Shaked S., Rieke M., Rieke G., 2001, ApJ, 547, 129
Reichard T. et al., 2003, AJ, 125, 1711
Rieke G., Low F. J., 1972, ApJ, 176, L95
Rieke G., Low F. J., 1975, ApJ, 200, L67
Rieke G., Cutri R. M., Black J. H., Kailey W. F., McAlary C. W., Lebofsky M. J., Elston R., 1985, ApJ, 290, 116
Rigon G. et al., 2003, MNRAS, 340, 191
Rigopoulou D., Spoon H., Genzel R., Lutz D., Moorwood A., Tran Q., 1999, AJ, 118, 2625
Rowan-Robinson M., Crawford J., 1989, MNRAS, 238, 523
Rupke D., Veilleux S., Sanders D., 2002, ApJ, 570, 588
Sanders D. B., Mirabel F., 1996, ARA&A, 34, 749
Sanders D. B., Scoville N., Soifer B., Young J., Danielson G., 1987, ApJ, 312, L5
Sanders D. B., Soifer B. T., Elias J. H., Madore B. F., Matthews K., Neugebauer G., Scoville N. Z., 1988a, ApJ, 325, 74
Sanders D. B., Soifer B. T., Elias J. H., Neugebauer G., Matthews K., 1988b, ApJ, 328, L35
Sanders D. B., Scoville N., Soifer B. T., 1991, ApJ, 370, 158
Scannapieco E., Broadhurst T., 2001, ApJ, 549, 28
Scannapieco E., Thacker R., Davies M., 2001, ApJ, 557, 605
Schmidt G., Miller J., 1985, ApJ, 290, 517
Schweizer F., 1980, ApJ, 237, 303
Schweizer F., 1982, ApJ, 252, 455
Scoville N. Z., Norman C., 1988, ApJ, 332, 163
Scoville N. Z., Norman C., 1995, ApJ, 451, 510
Scoville N. Z., Sargent A., Sanders D., Soifer B., 1991, ApJ, 366, L5
Sekiguchi K., 1987, ApJ, 316, 645
Smith P. S., Schmidt G., Allen R., Angel J., 1995, ApJ, 444, 146
Soifer B., Houck J., Neugebauer G., 1987, ARA&A, 25, 187
Soifer B. et al., 2000, AJ, 119, 509
Solomon P., Vaden Bout P., Guelin M., 2003, Nat, 426, 636
Sprayberry D., Foltz C., 1992, ApJ, 390, 39
Springel V., Di Mateo T., Hernquist L., 2005, ApJ, 620, L79
Strickland D., Stevens I., 2000, MNRAS, 314, 511
Suchkov A., Balsara D., Heckman T., Leitherer C., 1994, ApJ, 430, 511
Sulentic J., Marziani P., Dultzin-Hacyan D., 2000, ARA&A, 38, 521
Surace J., 1998, PhD thesis, Univ. Hawaii
Surace J., Sanders D. B., Vacca W. D., Veilleux S., Mazzarella J. M., 1998, ApJ, 492, 116
Tacconi L., Genzel R., Lutz D., Rigopoulou D., Backer A., Iserlohe C., Tecza M., 2002, ApJ, 580, 73
Taniguchi Y., Shioya K., 2000, ApJ, 532, L12
Taylor G., Silver C., Ulvestad J., Carrilli C., 1999, ApJ, 519, 185
Tenorio-Tagle G., Silich S., Kunth D., Terlevich E., Terlevich R., 1999, MNRAS, 309, 332
Terlevich R., Tenorio-Tagle G., Franco J., Melnick J., 1992, MNRAS, 255, 713
Terlevich R., Tenorio-Tagle G., Franco J., Boyle B., Rozyczka M., Melnick J., 1993, in Rocca-Volmerange B., Dennefeld M., Guiderdoni B., Tran Thanh Van J., eds, First Light in the Universe: Star or QSOs. Editions Frontieres, Gif-sur-Yvette, p. 261
Terlevich R., Fabian A., Turatto M., 1999, IAU Circ., 7269
Theuns T., Viel M., Kay S., Schaye J., Carswell R., Tzanavaris P., 2002, ApJ, 578, L5
Thorsett S., Hogg D., 1999, GCN Cir., 127
Toomre A., 1977, in Tinsley B., Larson R., eds, The Evolution of Galaxies and Stellar Population. Yale University Observatory, New Haven, p. 401
Toomre A., Toomre J., 1972, ApJ, 179, 623
Tomisaka K., Ikeuchi S., 1988, ApJ, 330, 695
Turner T., 1999, ApJ, 511, 142
Turnshek D., Monier E., Sirola C., Espey B., 1997, ApJ, 476, 40
Ulrich M., 1972, ApJ, 178, 113
Ulvestad J., Wrobel J., Carilli C., 1999a, ApJ, 516, 127
Ulvestad J., Wrobel J., Roy A., Wilson A., Falcke H., Krichbaun T., 1999b, ApJ, 517, L81
Vader J. P., 1986, ApJ, 305, 669
Vader J. P., 1987, ApJ, 317, 128
Veilleux S., Bland-Hawthorn J., 1997, ApJ, 479, L105
Veilleux S., Kim D., Sanders D., 1999, ApJ, 522, 113
Veilleux S., Cecil G., Bland-Hawthorn J., Tully R., Filippenko A., Sargent W., 1994, ApJ, 433, 48
Veilleux S., Cecil G., Bland-Hawthorn J., Shopell P., 2002a, in Henney W., Steffe W., Raga A., Binette L., eds, Emission Lines from Jets Flows, UNAM Mexico. RevMexAA Ser. Conf., 13, 222
Veilleux S., Kim D., Sanders D., 2002b, APJS, 143, 315
Voit G., Weymann R., Korista K., 1993, ApJ, 413, 95
Wampler E. J., 1985, ApJ, 296, 416
Wang Q., 1999, ApJ, 517, L27
Wang J., Heckman T., Weaver K., Armus L., 1997, ApJ, 474, 659
Weedman D., 1973, ApJ, 183, 29
Weymann R., Morris S., Foltz C., Hewitt P., 1991, ApJ, 373, 23
Zheng X., Xia X., Mao S., Deng Z., 2002, AJ, 124, 18

This paper has been typeset from a TEX/LATEX file prepared by the author.